12

Current Programmed Control

So far, we have discussed duty ratio control of PWM converters, in which the converter output is controlled by direct choice of the duty ratio $d(t)$. We have therefore developed expressions and small-signal transfer functions that relate the converter waveforms and output voltage to the duty ratio.

Another control scheme, which finds wide application, is current programmed control [1–13], in which the converter output is controlled by choice of the peak transistor switch current peak($i_s(t)$). The control input signal is a current $i_c(t)$, and a simple control network switches the transistor on and off, such that the peak transistor current follows $i_c(t)$. The transistor duty cycle $d(t)$ is not directly controlled, but depends on $i_c(t)$ as well as on the converter inductor currents, capacitor voltages, and power input voltage. Converters controlled via current programming are said to operate in the *current programmed mode* (CPM).

The block diagram of a simple current programmed controller is illustrated in Fig. 12.1. Control signal $i_c(t)$ and switch current $i_s(t)$ waveforms are given in Fig. 12.2. A clock pulse at the Set input of a latch initiates the switching period, causing the latch output Q to be high and turning on the transistor. While the transistor conducts, its current $i_s(t)$ is equal to the inductor current $i_L(t)$; this current increases with some positive slope m_1 that depends on the value of inductance and the converter voltages. In more complicated converters, $i_s(t)$ may follow the sum of several inductor currents. Eventually, the switch current $i_s(t)$ becomes equal to the control signal $i_c(t)$. At this point, the controller turns the transistor switch off, and the inductor current decreases for the remainder of the switching period. The controller must measure the switch current $i_s(t)$ with some current sensor circuit, and compare $i_s(t)$ to $i_c(t)$ using an analog comparator. In practice, voltages proportional to $i_s(t)$ and $i_c(t)$ are compared, with constant of proportionality R_f. When $i_s(t) \geq i_c(t)$, the comparator resets the latch, turning the transistor off for the remainder of the switching period.

As usual, a feedback loop can be constructed for regulation of the output voltage. The output voltage $v(t)$ is compared to a reference voltage v_{ref}, to generate an error signal. This error signal is applied

R. W. Erickson et al., *Fundamentals of Power Electronics*

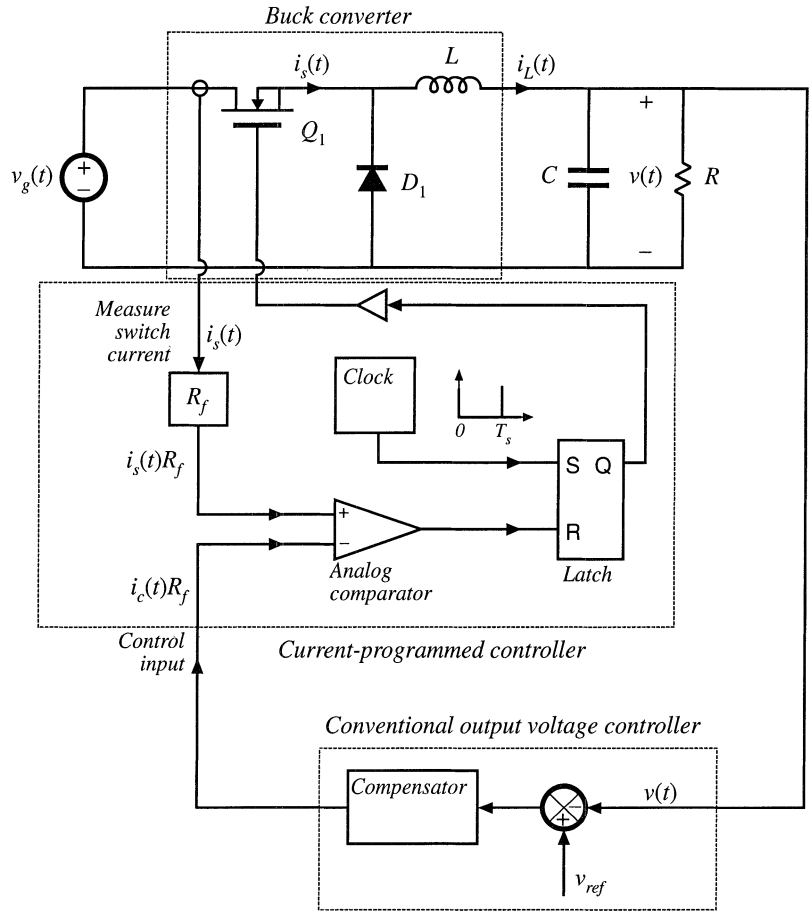

Fig. 12.1 Current-programmed control of a buck converter. The peak transistor current replaces the duty cycle as the control input.

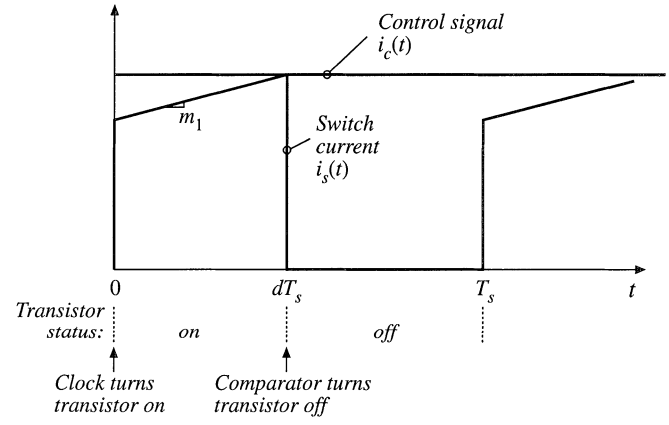

Fig. 12.2 Switch current $i_s(t)$ and control input $i_c(t)$ waveforms, for the current-programmed system ofFig. 12.1.

to the input of a compensation network, and the output of the compensator drives the control signal $i_c(t)R_f$. To design such a feedback system, we need to model how variations in the control signal $i_c(t)$ and in the line input voltage $v_g(t)$ affect the output voltage $v(t)$.

The chief advantage of the current programmed mode is its simpler dynamics. To first order, the small-signal control-to-output transfer function $\hat{v}(s)/\hat{i}_c(s)$ contains one less pole than $\hat{v}(s)/\hat{d}(s)$. Actually, this pole is moved to a high frequency, near the converter switching frequency. Nonetheless, simple robust wide-bandwidth output voltage control can usually be obtained, without the use of compensator lead networks. It is true that the current programmed controller requires a circuit for measurement of the switch current $i_s(t)$; however, in practice such a circuit is also required in duty ratio controlled systems, for protection of the transistor against excessive currents during transients and fault conditions. Current programmed control makes use of the available current sensor information during normal operation of the converter, to obtain simpler system dynamics. Transistor failures due to excessive switch current can then be prevented simply by limiting the maximum value of $i_c(t)$. This ensures that the transistor will turn off whenever the switch current becomes too large, on a cycle-by-cycle basis.

An added benefit is the reduction or elimination of transformer saturation problems in full-bridge or push–pull isolated converters. In these converters, small voltage imbalances induce a dc bias in the transformer magnetizing current; if sufficiently large, this dc bias can saturate the transformer. The dc current bias increases or decreases the transistor switch currents. In response, the current programmed controller alters the transistor duty cycles, such that transformer volt-second balance tends to be maintained. Current-programmed full-bridge isolated buck converters should be operated without a capacitor in series with the transformer primary winding; this capacitor tends to destabilize the system. For the same reason, current-programmed control of half-bridge isolated buck converters is generally avoided.

A disadvantage of current programmed control is its susceptibility to noise in the $i_s(t)$ or $i_c(t)$ signals. This noise can prematurely reset the latch, disrupting the operation of the controller. In particular, a small amount of filtering of the sensed switch current waveform is necessary, to remove the turn-on current spike caused by the diode stored charge. Addition of an artificial ramp to the current-programmed controller, as discussed in Section 12.1, can also improve the noise immunity of the circuit.

Commercial integrated circuits that implement current programmed control are widely available, and operation of converters in the current programmed mode is quite popular. In this chapter, converters operating in the current programmed mode are modeled. In Section 12.1, the stability of the current programmed controller and its inner switch-current-sensing loop is examined. It is found that this controller is unstable whenever converter steady-state duty cycle D is greater than 0.5. The current programmed controller can be stabilized by addition of an artificial ramp signal to the sensed switch current waveform. In Section 12.2, the system small-signal transfer functions are described, using a simple first-order model. The averaged terminal waveforms of the switch network can be described by a simple current source, in conjunction with a power source element. Perturbation and linearization leads to a simple small-signal model. Although this first-order model yields a great deal of insight into the control-to-output transfer function and converter output impedance, it does not predict the line-to-output transfer function $G_{vg}(s)$ of current-programmed buck converters. Hence, the model is refined in Section 12.3. Section 12.4 extends the modeling of current programmed converters to the discontinuous conduction mode.

12.1 OSCILLATION FOR $D > 0.5$

The current programmed controller of Fig. 12.1 is unstable whenever the steady-state duty cycle is greater than 0.5. To avoid this stability problem, the control scheme is usually modified, by addition of an artificial ramp to the sensed switch current waveform. In this section, the stability of the current programmed controller, with its inner switch-current-sensing loop, is analyzed. The effects of the addition of

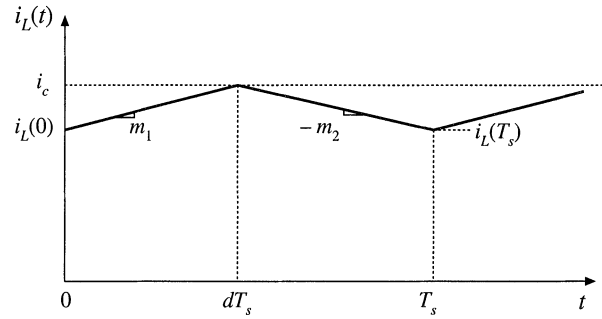

Fig. 12.3 Inductor current waveform of a current-programmed converter operating in the continuous conduction mode.

the artificial ramp are explained, using a simple first-order discrete-time analysis. Effects of the artificial ramp on controller noise susceptibility is also discussed.

Figure 12.3 illustrates a generic inductor current waveform of a switching converter operating in the continuous conduction mode. The inductor current changes with a slope m_1 during the first subinterval, and a slope $-m_2$ during the second subinterval. For the basic nonisolated converters, the slopes m_1 and $-m_2$ are given by

$$\begin{aligned}
&\text{Buck converter}\\
&m_1 = \frac{v_g - v}{L} \qquad -m_2 = -\frac{v}{L}\\
&\text{Boost converter}\\
&m_1 = \frac{v_g}{L} \qquad -m_2 = \frac{v_g - v}{L}\\
&\text{Buck–boost converter}\\
&m_1 = \frac{v_g}{L} \qquad -m_2 = \frac{v}{L}
\end{aligned} \tag{12.1}$$

With knowledge of the slopes m_1 and $-m_2$, we can determine the general relationships between $i_L(0)$, i_c, $i_L(T_s)$, and dT_s.

During the first subinterval, the inductor current $i_L(t)$ increases with slope m_1, until $i_L(t)$ reaches the control signal i_c. Hence,

$$i_L(dT_s) = i_c = i_L(0) + m_1 dT_s \tag{12.2}$$

Solution for the duty cycle d leads to

$$d = \frac{i_c - i_L(0)}{m_1 T_s} \tag{12.3}$$

In a similar manner, for the second subinterval we can write

$$\begin{aligned}
i_L(T_s) &= i_L(dT_s) - m_2 d'T_s\\
&= i_L(0) + m_1 dT_s - m_2 d'T_s
\end{aligned} \tag{12.4}$$

In steady-state, $i_L(0) = i_L(T_s)$, $d = D$, $m_1 = M_1$, and $m_2 = M_2$. Insertion of these relationships into Eq. (12.4) yields

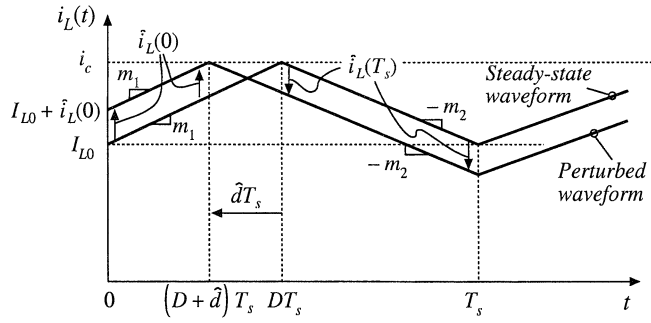

Fig. 12.4 Effect of initial perturbation $\hat{i}_L(0)$ on inductor current waveform.

$$0 = M_1 DT_s - M_2 D'T_s \tag{12.5}$$

Or,

$$\frac{M_2}{M_1} = \frac{D}{D'} \tag{12.6}$$

Steady-state Eq. (12.6) coincides with the requirement for steady-state volt-second balance on the inductor.

Consider now a small perturbation in $i_L(0)$:

$$i_L(0) = I_{L0} + \hat{i}_L(0) \tag{12.7}$$

I_{L0} is a steady-state value of $i_L(0)$, which satisfies Eqs. (12.4) and (12.5), while $\hat{i}_L(0)$ is a small perturbation such that

$$\left|\hat{i}_L(0)\right| \ll \left|I_{L0}\right| \tag{12.8}$$

It is desired to assess the stability of the current-programmed controller, by determining whether this small perturbation eventually decays to zero. To do so, let us solve for the perturbation after n switching periods, $\hat{i}_L(nT_s)$, and determine whether $\hat{i}_L(nT_s)$ tends to zero for large n.

The steady-state and perturbed inductor current waveforms are illustrated in Fig. 12.4. For clarity, the size of the inductor current perturbation $\hat{i}_L(0)$ is exaggerated. It is assumed that the converter operates near steady-state, such that the slopes m_1 and m_2 are essentially unchanged. Figure 12.4 is drawn for a positive $\hat{i}_L(0)$; the quantity $\hat{d}T_s$ is then negative. Since the slopes of the steady-state and perturbed waveforms are essentially equal over the interval $0 < t < (D + \hat{d})T_s$, the difference between the waveforms is equal to $\hat{i}_L(0)$ for this entire interval. Likewise, the difference between the two waveforms is a constant $\hat{i}_L(T_s)$ over the interval $DT_s < t < T_s$, since both waveforms then have the slope $-m_2$. Note that $\hat{i}_L(T_s)$ is a negative quantity, as sketched in Fig. 12.4. Hence, we can solve for $\hat{i}_L(T_s)$ in terms of $\hat{i}_L(0)$, by considering only the interval $(D + \hat{d})T_s < t < DT_s$ as illustrated in Fig. 12.5.

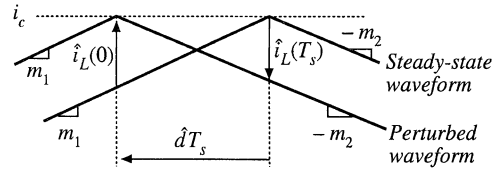

Fig. 12.5 Expanded view of the steady-state and perturbed inductor current waveforms, near the peak of $i_L(t)$.

From Fig. 12.5, we can use the steady-state waveform to express $\hat{i}_L(0)$ as the slope m_1, multiplied by the interval length $-\hat{d}T_s$. Hence,

$$\hat{i}_L(0) = -m_1 \hat{d} T_s \tag{12.9}$$

Likewise, we can use the perturbed waveform to express $\hat{i}_L(T_s)$ as the slope $-m_2$, multiplied by the interval length $-\hat{d}T_s$:

$$\hat{i}_L(T_s) = m_2 \hat{d} T_s \tag{12.10}$$

Elimination of the intermediate variable $\hat{d}$ from Eqs. (12.9) and (12.10) leads to

$$\hat{i}_L(T_s) = \hat{i}_L(0) \left(-\frac{m_2}{m_1} \right) \tag{12.11}$$

If the converter operating point is sufficiently close to the quiescent operating point, then m_2/m_1 is given approximately by Eq. (12.6). Equation (12.11) then becomes

$$\hat{i}_L(T_s) = \hat{i}_L(0) \left(-\frac{D}{D'} \right) \tag{12.12}$$

A similar analysis can be performed during the next switching period, to show that

$$\hat{i}_L(2T_s) = \hat{i}_L(T_s) \left(-\frac{D}{D'} \right) = \hat{i}_L(0) \left(-\frac{D}{D'} \right)^2 \tag{12.13}$$

After n switching periods, the perturbation becomes

$$\hat{i}_L(nT_s) = \hat{i}_L((n-1)T_s) \left(-\frac{D}{D'} \right) = \hat{i}_L(0) \left(-\frac{D}{D'} \right)^n \tag{12.14}$$

Note that, as n tends to infinity, the perturbation $\hat{i}_L(nT_s)$ tends to zero provided that the characteristic value $-D/D'$ has magnitude less than one. Conversely, the perturbation $\hat{i}_L(nT_s)$ becomes large in magnitude when the characteristic value $\alpha = -D/D'$ has magnitude greater than one:

$$\left| \hat{i}_L(nT_s) \right| \rightarrow \begin{cases} 0 & \text{when } \left| -\frac{D}{D'} \right| < 1 \\ \infty & \text{when } \left| -\frac{D}{D'} \right| > 1 \end{cases} \tag{12.15}$$

Therefore, for stable operation of the current programmed controller, we need $|\alpha| = D/D' < 1$, or

$$D < 0.5 \tag{12.16}$$

As an example, consider the operation of the boost converter with the steady-state terminal voltages $V_g = 20$ V, $V = 50$ V. Since $V/V_g = 1/D'$, the boost converter should operate with $D = 0.6$. We therefore expect the current programmed controller to be unstable. The characteristic value will be

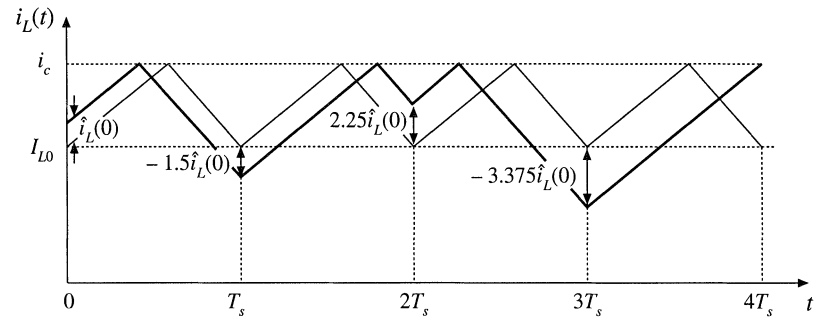

Fig. 12.6 Unstable oscillation for $D = 0.6$.

$$\alpha = -\frac{D}{D'} = \left(-\frac{0.6}{0.4}\right) = -1.5 \tag{12.17}$$

As given by Eq. (12.14), a perturbation in the inductor current will increase by a factor of – 1.5 over every switching period. As illustrated in Fig. 12.6, the perturbation grows to $-1.5\hat{i}_L(0)$ after one switching period, to $+2.25\hat{i}_L(0)$ after two switching periods, and to $-3.375\hat{i}_L(0)$ after three switching periods. For the particular initial conditions illustrated in Fig. 12.6, this growing oscillation saturates the current programmed controller after three switching periods. The transistor remains on for the entire duration of the fourth switching period. The inductor current and controller waveforms may eventually become oscillatory and periodic in nature, with period equal to an integral number of switching periods. Alternatively, the waveforms may become chaotic. In either event, the controller does not operate as intended.

Figure 12.7 illustrates the inductor current waveforms when the output voltage is decreased to $V = 30$ V. The boost converter then operates with $D = 1/3$, and the characteristic value becomes

$$\alpha = -\frac{D}{D'} = \left(-\frac{1/3}{2/3}\right) = -0.5 \tag{12.18}$$

Perturbations now decrease in magnitude by a factor of 0.5 over each switching period. A disturbance in the inductor current becomes small in magnitude after a few switching periods.

The instability for $D > 0.5$ is a well-known problem of current programmed control, which is not dependent on the converter topology. The controller can be rendered stable for all duty cycles by addition of an artificial ramp to the sensed switch current waveform, as illustrated in Fig. 12.8. This arti-

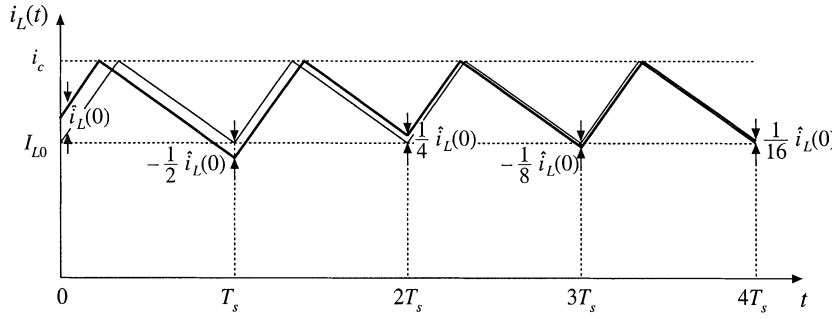

Fig. 12.7 A stable transient with $D = 1/3$.

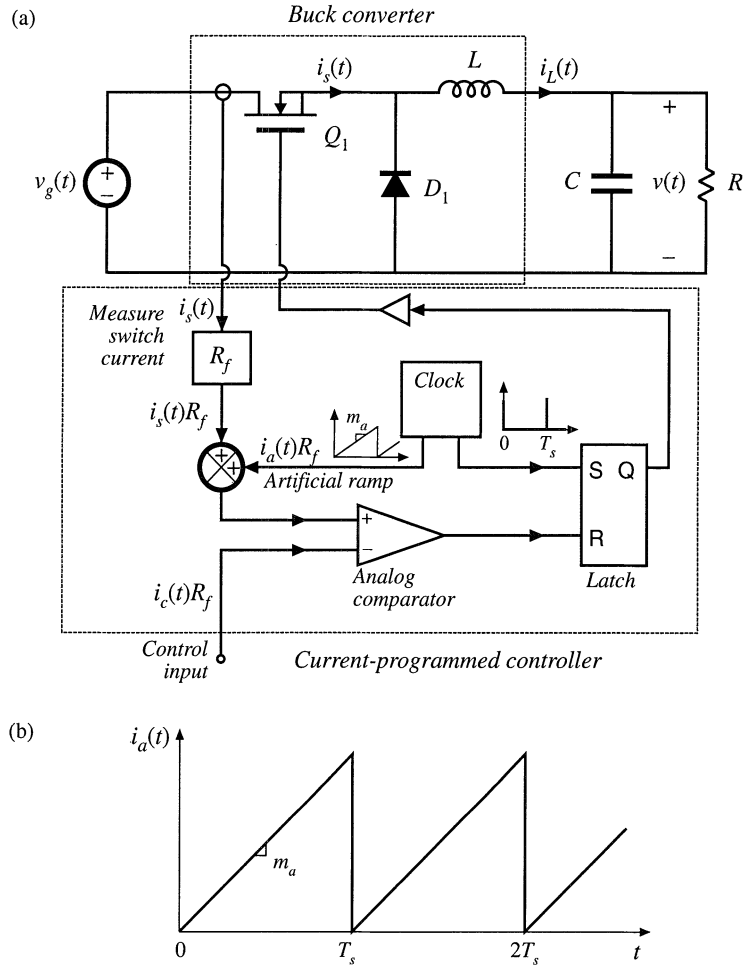

Fig. 12.8 Stabilization of the current programmed controller by addition of an artificial ramp to the measured switch current waveform: (a) block diagram, (b) artificial ramp waveform.

ficial ramp has the qualitative effect of reducing the gain of the inner switch-current-sensing discrete feedback loop. The artificial ramp has slope m_a as shown. The controller now switches the transistor off when

$$i_a(dT_s) + i_L(dT_s) = i_c \tag{12.19}$$

where $i_a(t)$ is the artificial ramp waveform. Therefore, the transistor is switched off when the inductor current $i_L(t)$ is given by

$$i_L(dT_s) = i_c - i_a(dT_s) \tag{12.20}$$

Figure 12.9 illustrates the analog comparison of the inductor current waveform $i_L(t)$ with the quantity $[i_c - i_a(t)]$.

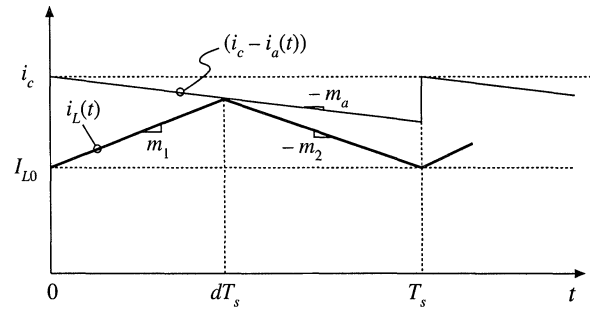

Fig. 12.9 Addition of artificial ramp: the transistor is now switched off when $i_L(t) = i_c - i_a(t)$.

We can again determine the stability of the current programmed controller by analyzing the change in a perturbation of the inductor current waveform over a complete switching period. Figure 12.10 illustrates steady-state and perturbed inductor current waveforms, in the presence of the artificial ramp. Again, the magnitude of the perturbation $\hat{i}_L(0)$ is exaggerated. The perturbed waveform is sketched for a positive value of $\hat{i}_L(0)$; this causes $\hat{d}$, and usually also $\hat{i}_L(T_s)$, to be negative. If the perturbed waveforms are sufficiently close to the quiescent operating point, then the slopes m_1 and m_2 are essentially unchanged, and the relationship between $\hat{i}_L(0)$ and $\hat{i}_L(T_s)$ can be determined solely by consideration of the interval $(D + \hat{d})T_s < t < DT_s$. The perturbations $\hat{i}_L(0)$ and $\hat{i}_L(T_s)$ are expressed in terms of the slopes m_1, m_2, and m_a, and the interval length $-\hat{d}T_s$, as follows:

$$\hat{i}_L(0) = -\hat{d}T_s\left(m_1 + m_a\right) \tag{12.21}$$

$$\hat{i}_L(T_s) = -\hat{d}T_s\left(m_a - m_2\right) \tag{12.22}$$

Elimination of $\hat{d}$ yields

$$\hat{i}_L(T_s) = \hat{i}_L(0)\left(-\frac{m_2 - m_a}{m_1 + m_a}\right) \tag{12.23}$$

A similar analysis can be applied to the n^{th} switching period, leading to

$$\hat{i}_L(nT_s) = \hat{i}_L((n-1)T_s)\left(-\frac{m_2 - m_a}{m_1 + m_a}\right) = \hat{i}_L(0)\left(-\frac{m_2 - m_a}{m_1 + m_a}\right)^n = \hat{i}_L(0)\,\alpha^n \tag{12.24}$$

The evolution of inductor current perturbations are now determined by the characteristic value

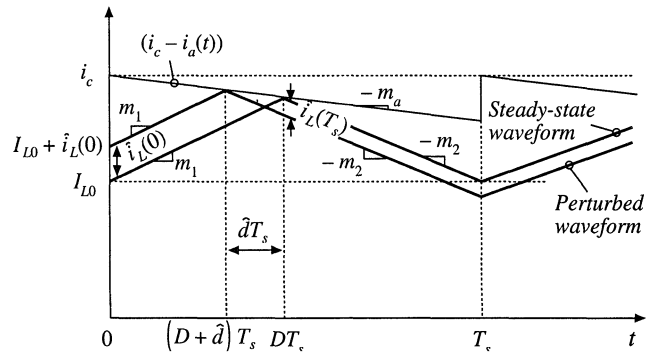

Fig. 12.10 Steady-state and perturbed inductor current waveforms, in the presence of an artificial ramp.

$$\alpha = -\frac{m_2 - m_a}{m_1 + m_a} \tag{12.25}$$

For large n, the perturbation magnitude tends to

$$\left|\hat{i}_L(nT_s)\right| \rightarrow \begin{cases} 0 & \text{when } |\alpha| < 1 \\ \infty & \text{when } |\alpha| > 1 \end{cases} \tag{12.26}$$

Therefore, for stability of the current programmed controller, we need to choose the slope of the artificial ramp m_a such that the characteristic value α has magnitude less than one. The artificial ramp gives us an additional degree of freedom, which we can use to stabilize the system for duty cycles greater than 0.5. Note that increasing the value of m_a causes the numerator of Eq. (12.25) to decrease, while the denominator increases. Therefore, the characteristic value α attains magnitude less than one for sufficiently large m_a.

In the conventional voltage regulator application, the output voltage $v(t)$ is well regulated by the converter control system, while the input voltage $v_g(t)$ is unknown. Equation (12.1) then predicts that the value of the slope m_2 is constant and known with a high degree of accuracy, for the buck and buck-boost converters. Therefore, let us use Eq. (12.6) to eliminate the slope m_1 from Eq. (12.25), and thereby express the characteristic value α as a function of the known slope m_2 and the steady-state duty cycle D:

$$\alpha = -\frac{1 - \frac{m_a}{m_2}}{\frac{D'}{D} + \frac{m_a}{m_2}} \tag{12.27}$$

One common choice of artificial ramp slope is

$$m_a = \tfrac{1}{2} m_2 \tag{12.28}$$

It can be verified, by substitution of Eq. (12.28) into (12.27), that this choice leads to $\alpha = -1$ at $D = 1$, and to $|\alpha| < 1$ for $0 \leq D < 1$. This is the minimum value of m_a that leads to stability for all duty cycles. We will see in Section 12.3 that this choice of m_a has the added benefit of causing the ideal line-to-output transfer function $G_{vg}(s)$ of the buck converter to become zero.

Another common choice of m_a is

$$m_a = m_2 \tag{12.29}$$

This causes the characteristic value α to become zero for all D. As a result, $\hat{i}_L(T_s)$ is zero for any $\hat{i}_L(0)$ that does not saturate the controller. The system removes any error after one switching period T_s. This behavior is known as *deadbeat control*, or *finite settling time*.

It should be noted that the above stability analysis employs a quasi-static approximation, in which the slopes m_1 and m_2 of the perturbed inductor current waveforms are assumed to be identical to the steady-state case. In the most general case, the stability and transient response of a complete system employing current programmed control must be assessed using a system-wide discrete time or sampled-data analysis. Nonetheless, in practice the above arguments are found to be sufficient for selection of the artificial ramp slope m_a.

Current-programmed controller circuits exhibit significant sensitivity to noise. The reason for this is illustrated in Fig. 12.11(a), in which the control signal $i_c(t)$ is perturbed by a small amount of noise

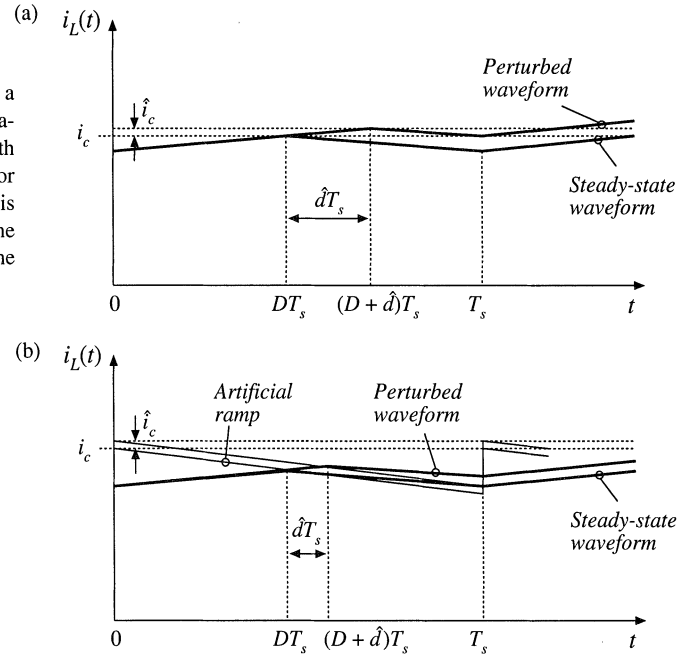

Fig. 12.11 When noise perturbs a controller signal such as i_c, a perturbation in the duty cycle results: (a) with no artificial ramp and small inductor current ripple, the perturbation $\hat{d}$ is large; (b) an artificial ramp reduces the controller gain, thereby reducing the perturbation $\hat{d}$.

represented by $\hat{i}_c$. It can be seen that, when there is no artificial ramp and when the inductor current ripple is small, then a small perturbation in i_c leads to a large perturbation in the duty cycle: the controller has high gain. When noise is present in the controller circuit, then significant jitter in the duty cycle waveforms may be observed. A solution is to reduce the gain of the controller by introduction of an artificial ramp. As illustrated in Fig. 12.11(b), the same perturbation in i_c now leads to a reduced variation in the duty cycle. When the layout and grounding of the controller circuit introduce significant noise into the duty cycle waveform, it may be necessary to add an artificial ramp whose amplitude is substantially greater than the inductor current ripple.

12.2 A SIMPLE FIRST-ORDER MODEL

Once the current programmed controller has been constructed, and stabilized using an artificial ramp, then it is desired to design a feedback loop for regulation of the output voltage. As usual, this voltage feedback loop must be designed to meet specifications regarding line disturbance rejection, transient response, output impedance, etc. A block diagram of a typical system is illustrated in Fig. 12.12, containing an inner current programmed controller, with an outer voltage feedback loop.

To design the outer voltage feedback loop, an ac equivalent circuit model of the switching converter operating in the current programmed mode is needed. In Chapter 7, averaging was employed to develop small-signal ac equivalent circuit models for converters operating with duty ratio control. These models predict the circuit behavior in terms of variations d in the duty cycle. If we could find the relationship between the control signal $i_c(t)$ and the duty cycle $d(t)$ for the current programmed controller, then we could adapt the models of Chapter 7, to apply to the current programmed mode as well. In general, the duty cycle depends not only on $i_c(t)$, but also on the converter voltages and currents; hence, the current programmed controller incorporates multiple effective feedback loops as indicated in Fig. 12.12.

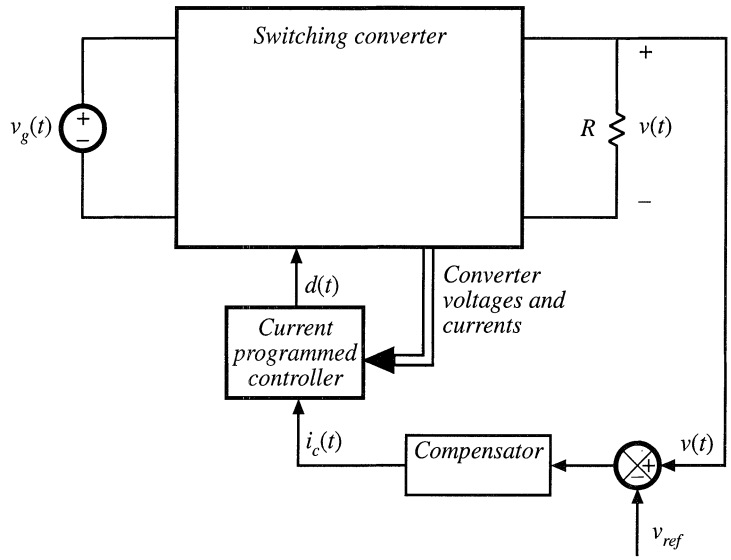

Fig. 12.12 Block diagram of a converter system incorporating current programmed control.

In this section, the averaging approach is extended, as described above, to treat current programmed converters. A simple first-order approximation is employed, in which it is assumed that the current programmed controller operates ideally, and hence causes the average inductor current $\langle i_L(t) \rangle_{T_s}$ to be identical to the control $i_c(t)$. This approximation is justified whenever the inductor current ripple and artificial ramp have negligible magnitudes. The inductor current then is no longer an independent state of the system, and no longer contributes a pole to the converter small-signal transfer functions.

This first-order model is derived in Section 12.2.1, using a simple algebraic approach. In Section 12.2.2, a simple physical interpretation is obtained via the averaged switch modeling technique. A more accurate, but more complicated, model is described in Section 12.3.

12.2.1 Simple Model via Algebraic Approach: Buck-Boost Example

The power stage of a simple buck-boost converter operating in the continuous conduction mode is illustrated in Fig. 12.13(a), and its inductor current waveform is given in Fig. 12.13(b). The small-signal averaged equations for this converter, under duty cycle control, were derived in Section 7.2. The result, Eq. (7.43), is reproduced below:

$$\begin{aligned} L\frac{d\hat{i}_L(t)}{dt} &= D\hat{v}_g(t) + D'\hat{v}(t) + \left(V_g - V\right)\hat{d}(t) \\ C\frac{d\hat{v}(t)}{dt} &= -D'\hat{i}_L - \frac{\hat{v}(t)}{R} + I_L\hat{d}(t) \\ \hat{i}_g(t) &= D\hat{i}_L + I_L\hat{d}(t) \end{aligned} \tag{12.30}$$

The Laplace transforms of these equations, with initial conditions set to zero, are

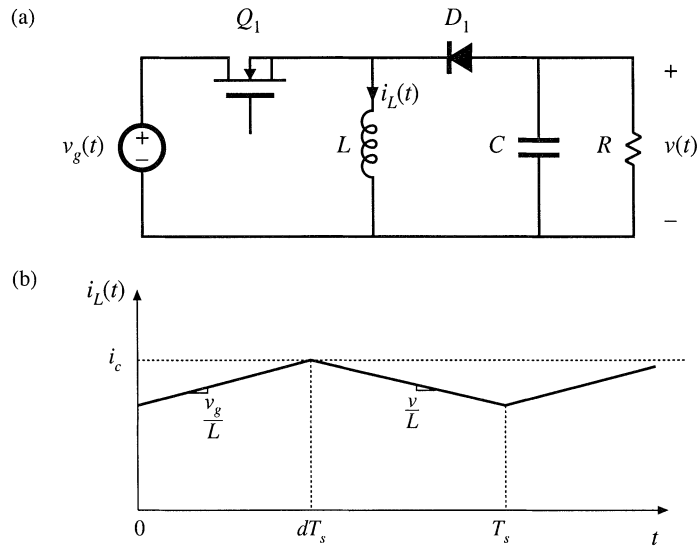

Fig. 12.13 Buck-boost converter example: (a) power stage, (b) inductor current waveform.

$$\begin{aligned} sL\hat{i}_L(s) &= D\hat{v}_g(s) + D'\hat{v}(s) + \left(V_g - V\right)\hat{d}(s) \\ sC\hat{v}(s) &= -D'\hat{i}_L(s) - \frac{\hat{v}(s)}{R} + I_L\hat{d}(s) \\ \hat{i}_g(s) &= D\hat{i}_L(s) + I_L\hat{d}(s) \end{aligned} \tag{12.31}$$

We now make the assumption that the inductor current $\hat{i}_L(s)$ is identical to the programmed control current $\hat{i}_c(s)$. This is valid to the extent that the controller is stable, and that the magnitudes of the inductor current ripple and artificial ramp waveform are sufficiently small:

$$\hat{i}_L(s) \approx \hat{i}_c(s) \tag{12.32}$$

This approximation, in conjunction with the inductor current equation of (12.31), can now be used to find the relationship between the control current $\hat{i}_c(s)$ and the duty cycle $\hat{d}(s)$, as follows:

$$sL\hat{i}_c(s) \approx D\hat{v}_g(s) + D'\hat{v}(s) + \left(V_g - V\right)\hat{d}(s) \tag{12.33}$$

Solution for $\hat{d}(s)$ yields

$$\hat{d}(s) = \frac{sL\hat{i}_c(s) - D\hat{v}_g(s) - D'\hat{v}(s)}{\left(V_g - V\right)} \tag{12.34}$$

This small-signal expression describes how the current programmed controller varies the duty cycle, in response to a given control input variation $\hat{i}_c(s)$. It can be seen that $\hat{d}(s)$ depends not only on $\hat{i}_c(s)$, but also on the converter output voltage and input voltage variations. Equation (12.34) can now be substituted into the second and third lines of Eq. (12.31), thereby eliminating $\hat{d}(s)$. One obtains

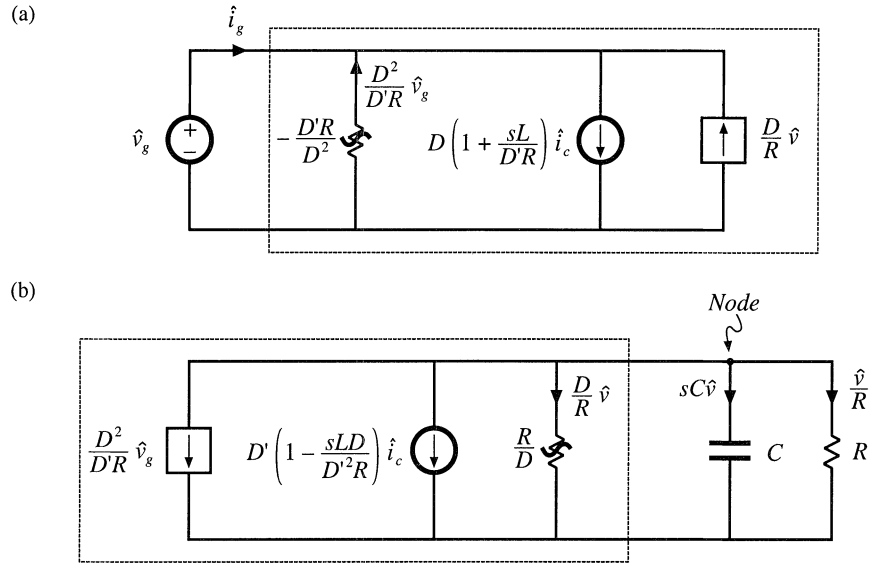

Fig. 12.14 Construction of CPM CCM buck–boost converter equivalent circuit: (a) input port model, corresponding to Eq. (12.38); (b) output port model, corresponding to Eq. (12.37).

$$\begin{aligned} sC\hat{v}(s) &= -D'\hat{i}_c(s) - \frac{\hat{v}(s)}{R} + I_L \frac{sL\hat{i}_c(s) - D\hat{v}_g(s) - D'\hat{v}(s)}{\left(V_g - V\right)} \\ \hat{i}_g(s) &= D\hat{i}_c(s) + I_L \frac{sL\hat{i}_c(s) - D\hat{v}_g(s) - D'\hat{v}(s)}{\left(V_g - V\right)} \end{aligned} \tag{12.35}$$

These equations can be simplified by collecting terms, and by use of the steady-state relationships

$$\begin{aligned} V &= -\frac{D}{D'} V_g \\ I_L &= -\frac{V}{D'R} = \frac{D}{D'^2R} V_g \end{aligned} \tag{12.36}$$

Equation (12.35) then becomes

$$sC\hat{v}(s) = \left(\frac{sLD}{D'R} - D'\right)\hat{i}_c(s) - \left(\frac{D}{R} + \frac{1}{R}\right)\hat{v}(s) - \left(\frac{D^2}{D'R}\right)\hat{v}_g(s) \tag{12.37}$$

$$\hat{i}_g(s) = \left(\frac{sLD}{D'R} + D\right)\hat{i}_c(s) - \left(\frac{D}{R}\right)\hat{v}(s) - \left(\frac{D^2}{D'R}\right)\hat{v}_g(s) \tag{12.38}$$

These are the basic ac small-signal equations for the simplified first-order model of the current-programmed buck-boost converter. These equations can now be used to construct small-signal ac circuit models that represent the behavior of the converter input and output ports. In Eq. (12.37), the quantity $sC\hat{v}(s)$ is the output capacitor current. The $\hat{i}_c(s)$ term is represented in Fig. 12.14(b) by an independent

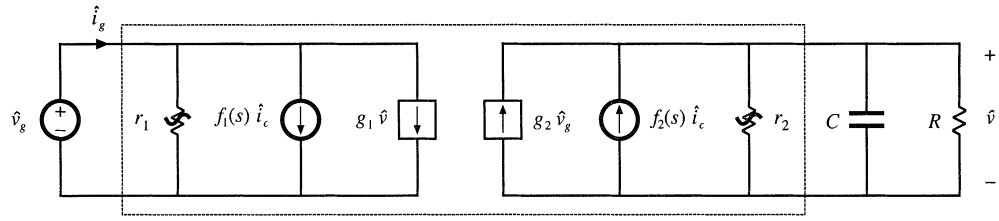

Fig. 12.15 Two-port equivalent circuit used to model the current-programmed CCM buck, boost, and buck–boost converters.

current source, while the $\hat{v}_g(s)$ term is represented by a dependent current source. $\hat{v}(s)/R$ is the current through the load resistor, and $\hat{v}(s)D/R$ is the current through an effective ac resistor of value R/D.

Equation (12.38) describes the current $\hat{i}_g(s)$ drawn by the converter input port, out of the source $\hat{v}_g(s)$. The $\hat{i}_c(s)$ term is again represented in Fig. 12.14(a) by an independent current source, and the $\hat{v}(s)$ term is represented by a dependent current source. The quantity $-\hat{v}_g(s)D^2/D'R$ is modeled by an effective ac resistor having the negative value $-D'R/D^2$.

Figures 12.14(a) and (b) can now be combined into the small-signal two-port model of Fig. 12.15. The current programmed buck and boost converters can also be modeled by a two-port equivalent circuit, of the same form. Table 12.1 lists the model parameters for the basic buck, boost, and buck-boost converters.

The two-port equivalent circuit can now be solved, to find the converter transfer functions and output impedance. The control-to-output transfer function is found by setting v_g to zero. Solution for the output voltage then leads to the transfer function $G_{vc}(s)$:

$$G_{vc}(s) = \left.\frac{\hat{v}(s)}{\hat{i}_c(s)}\right|_{\hat{v}_g = 0} = f_2\left(r_2 \,\|\, R \,\|\, \frac{1}{sC}\right) \tag{12.39}$$

Substitution of the model parameters for the buck-boost converter yields

$$G_{vc}(s) = -R\,\frac{D'}{1+D}\,\frac{\left(1 - s\,\frac{DL}{D'^2R}\right)}{\left(1 + s\,\frac{RC}{1+D}\right)} \tag{12.40}$$

Table 12.1 Current programmed mode small-signal equivalent circuit parameters, simple model

Converter	g_1	f_1	r_1	g_2	f_2	r_2
Buck	$\frac{D}{R}$	$D\left(1 + \frac{sL}{R}\right)$	$-\frac{R}{D^2}$	0	1	∞
Boost	0	1	∞	$\frac{1}{D'R}$	$D'\left(1 - \frac{sL}{D'^2R}\right)$	R
Buck–boost	$-\frac{D}{R}$	$D\left(1 + \frac{sL}{D'R}\right)$	$-\frac{D'R}{D^2}$	$-\frac{D^2}{D'R}$	$-D'\left(1 - \frac{sDL}{D'^2R}\right)$	$\frac{R}{D}$

It can be seen that this transfer function contains only one pole; the pole due to the inductor has been lost. The dc gain is now directly dependent on the load resistance R. In addition, the transfer function contains a right half-plane zero whose corner frequency is unchanged from the duty-cycle-controlled case. In general, introduction of current programming alters the transfer function poles and dc gain, but not the zeroes.

The line-to-output transfer function $G_{vg}(s)$ is found by setting the control input i_c to zero, and then solving for the output voltage. The result is

$$G_{vg}(s) = \left.\frac{\hat{v}(s)}{\hat{v}_g(s)}\right|_{i_c=0} = g_2\left(r_2 \parallel R \parallel \frac{1}{sC}\right) \tag{12.41}$$

Substitution of the parameters for the buck-boost converter leads to

$$G_{vg}(s) = -\frac{D^2}{1-D^2}\frac{1}{\left(1+s\frac{RC}{1+D}\right)} \tag{12.42}$$

Again, the inductor pole is lost. The output impedance is

$$Z_{out}(s) = r_2 \parallel R \parallel \frac{1}{sC} \tag{12.43}$$

For the buck-boost converter, one obtains

$$Z_{out}(s) = \frac{R}{1+D}\frac{1}{\left(1+s\frac{RC}{1+D}\right)} \tag{12.44}$$

12.2.2 Averaged Switch Modeling

Additional physical insight into the properties of current programmed converters can be obtained by use of the averaged switch modeling approach developed in Section 7.4. Consider the buck converter of Fig. 12.16. We can define the terminal voltages and currents of the switch network as shown. When the buck converter operates in the continuous conduction mode, the switch network average terminal waveforms are related as follows:

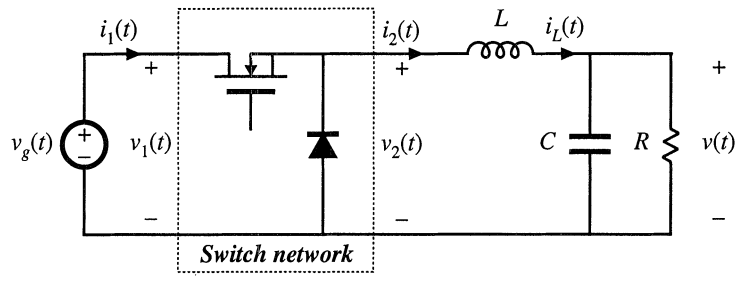

Fig. 12.16 Averaged switch modeling of a current-programmed converter: CCM buck example.

$$\begin{aligned} \langle v_2(t)\rangle_{T_s} &= d(t)\,\langle v_1(t)\rangle_{T_s} \\ \langle i_1(t)\rangle_{T_s} &= d(t)\,\langle i_2(t)\rangle_{T_s} \end{aligned} \tag{12.45}$$

We again invoke the approximation in which the inductor current exactly follows the control current. In terms of the switch network terminal current i_2, we can therefore write

$$\langle i_2(t)\rangle_{T_s} \approx \langle i_c(t)\rangle_{T_s} \tag{12.46}$$

The duty cycle $d(t)$ can now be eliminated from Eq. (12.45), as follows:

$$\langle i_1(t)\rangle_{T_s} = d(t)\,\langle i_c(t)\rangle_{T_s} = \frac{\langle v_2(t)\rangle_{T_s}}{\langle v_1(t)\rangle_{T_s}}\,\langle i_c(t)\rangle_{T_s} \tag{12.47}$$

This equation can be written in the alternative form

$$\langle i_1(t)\rangle_{T_s}\,\langle v_1(t)\rangle_{T_s} = \langle i_c(t)\rangle_{T_s}\,\langle v_2(t)\rangle_{T_s} = \langle p(t)\rangle_{T_s} \tag{12.48}$$

Equations (12.46) and (12.48) are the desired result, which describes the average terminal relations of the CCM current-programmed buck switch network. Equation (12.46) states that the average terminal current $\langle i_2(t)\rangle_{T_s}$ is equal to the control current $\langle i_c(t)\rangle_{T_s}$. Equation (12.48) states that the input port of the switch network consumes average power $\langle p(t)\rangle_{T_s}$ equal to the average power flowing out of the switch output port. The averaged equivalent circuit of Fig. 12.17 is obtained.

Figure 12.17 describes the behavior of the current programmed buck converter switch network, in a simple and straightforward manner. The switch network output port behaves as a current source of value $\langle i_c(t)\rangle_{T_s}$. The input port follows a power sink characteristic, drawing power from the source v_g equal to the power supplied by the i_c current source. Properties of the power source and power sink elements are described in Chapters 11 and 18.

Similar arguments lead to the averaged switch models of the current programmed boost and buck-boost converters, illustrated in Fig. 12.18. In both cases, the switch network averaged terminal waveforms can be represented by a current source of value $\langle i_c(t)\rangle_{T_s}$, in conjunction with a dependent power source or power sink.

A small-signal ac model of the current-programmed buck converter can now be constructed by perturbation and linearization of the switch network averaged terminal waveforms. Let

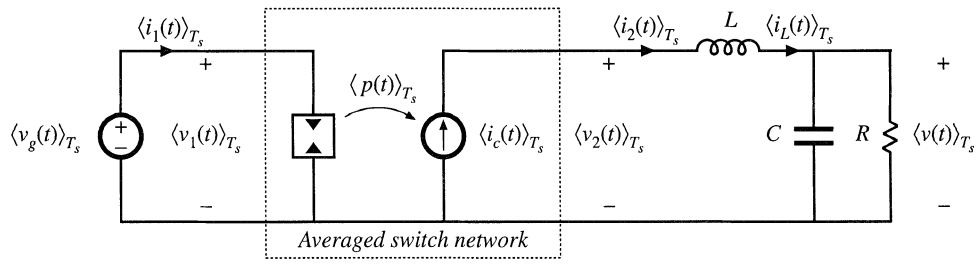

Fig. 12.17 Averaged model of CPM buck converter.

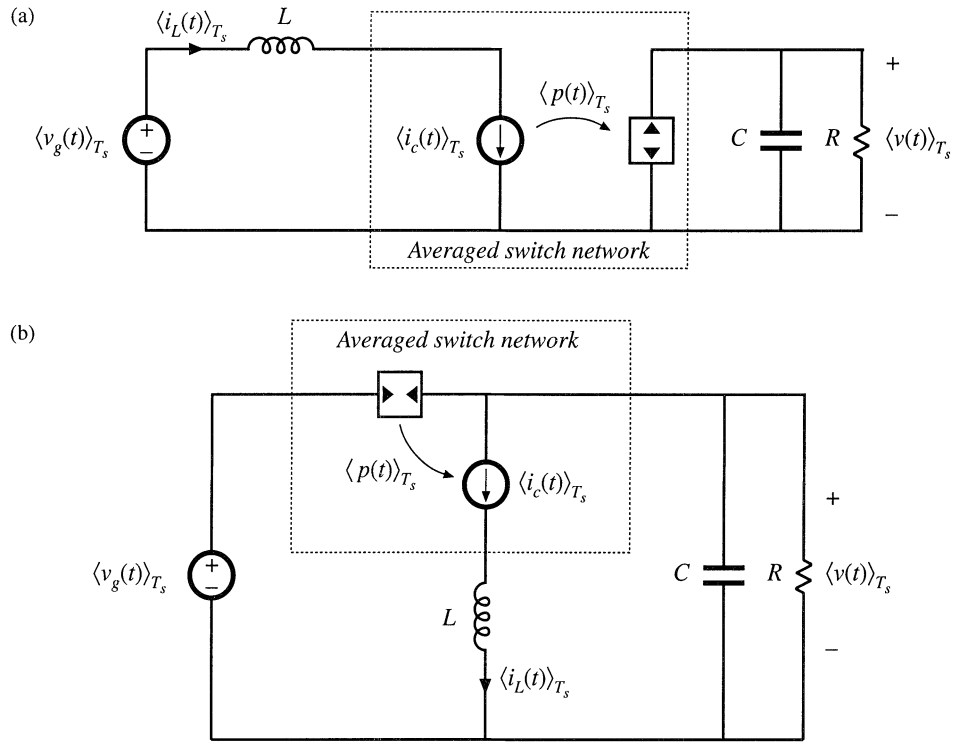

Fig. 12.18 Averaged models of CPM boost (a) and CPM buck–boost (b) converters, derived via averaged switch modeling.

$$\begin{aligned}
\langle v_1(t)\rangle_{T_s} &= V_1 + \hat{v}_1(t) \\
\langle i_1(t)\rangle_{T_s} &= I_1 + \hat{i}_1(t) \\
\langle v_2(t)\rangle_{T_s} &= V_2 + \hat{v}_2(t) \\
\langle i_2(t)\rangle_{T_s} &= I_2 + \hat{i}_2(t) \\
\langle i_c(t)\rangle_{T_s} &= I_c + \hat{i}_c(t)
\end{aligned} \tag{12.49}$$

Perturbation and linearization of the $\langle i_c(t)\rangle_{T_s}$ current source of Fig. 12.17 simply leads to a current source of value $\hat{i}_c(t)$. Perturbation of the power source characteristic, Eq. (12.48), leads to

$$\left(V_1 + \hat{v}_1(t)\right)\left(I_1 + \hat{i}_1(t)\right) = \left(I_c + \hat{i}_c(t)\right)\left(V_2 + \hat{v}_2(t)\right) \tag{12.50}$$

Upon equating the dc terms on both sides of this equation, we obtain

$$V_1 I_1 = I_c V_2 \quad \Rightarrow \quad I_1 = D I_c \tag{12.51}$$

The linear small-signal ac terms of Eq. (12.50) are

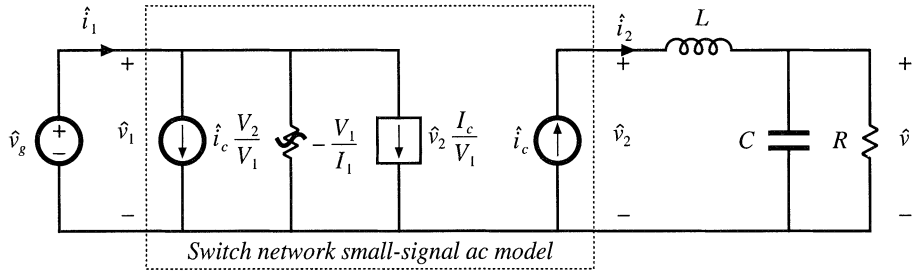

Fig. 12.19 Small-signal model of the CCM CPM buck converter, derived by perturbation and linearization of the switch network in Fig. 12.17.

$$\hat{v}_1(t)I_1 + V_1\hat{i}_1(t) = \hat{i}_c(t)V_2 + I_c\hat{v}_2(t) \tag{12.52}$$

Solution for the small-signal switch network input current $\hat{i}_1(t)$ yields

$$\hat{i}_1(t) = \hat{i}_c(t)\frac{V_2}{V_1} + \hat{v}_2(t)\frac{I_c}{V_1} - \hat{v}_1(t)\frac{I_1}{V_1} \tag{12.53}$$

The small-signal ac model of Fig. 12.19 can now be constructed. The switch network output port is again a current source, of value $\hat{i}_c(t)$. The switch network input port model is obtained by linearization of the power sink characteristic, as given by Eq. (12.53). The input port current $\hat{i}_1(t)$ is composed of three terms. The $\hat{i}_c(t)$ term is modeled by an independent current source, the $\hat{v}_2(t)$ term is modeled by a dependent current source, and the $\hat{v}_1(t)$ term is modeled by an effective ac resistor having the negative value $-V_1/I_1$. As illustrated in Fig. 12.20, this incremental resistance is determined by the slope of the power sink input port characteristic, evaluated at the quiescent operating point. The power sink leads to a negative incremental resistance because an increase in $\langle v_1(t)\rangle_{T_s}$ causes a decrease in $\langle i_1(t)\rangle_{T_s}$, such that constant $\langle p(t)\rangle_{T_s}$ is maintained.

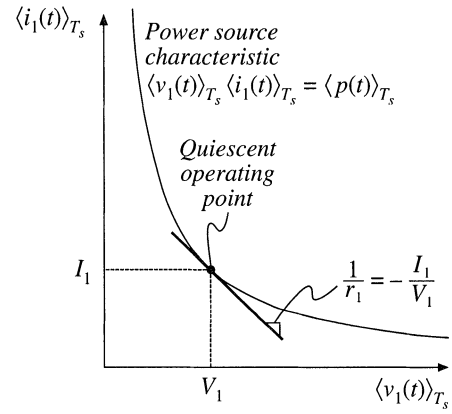

Fig. 12.20 Origin of the input port negative incremental resistance r_1: the slope of the power sink characteristic, evaluated at the quiescent operating point.

The equivalent circuit of Fig. 12.19 can now be simplified by use of the dc relations $V_2 = DV_1$, $I_2 = V_2/R$, $I_1 = DI_2$, $I_2 = I_c$. Equation (12.53) then becomes

$$\hat{i}_1(t) = D\hat{i}_c(t) + \frac{D}{R}\hat{v}_2(t) - \frac{D^2}{R}\hat{v}_1(t) \tag{12.54}$$

Finally, we can eliminate the quantities $\hat{v}_1$ and $\hat{v}_2$ in favor of the converter terminal voltages $\hat{v}_g$ and $\hat{v}$, as follows. The quantity $\hat{v}_1$ is simply equal to $\hat{v}_g$. The quantity $\hat{v}_2$ is equal to the output voltage $\hat{v}$ plus the voltage across the inductor, $sL\hat{i}_c(s)$. Hence,

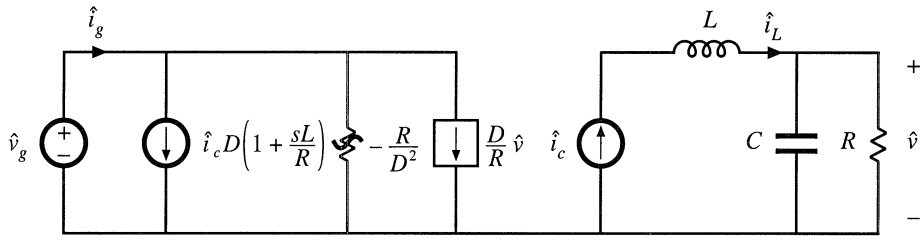

Fig. 12.21 Simplification of the CPM buck converter model of Fig. 12.19, with dependent source expressed in terms of the output voltage variations.

$$\hat{v}_2(s) = \hat{v}(s) + sL\hat{i}_c(s) \tag{12.55}$$

With these substitutions, Eq. (12.54) becomes

$$\hat{i}_1(s) = D\left(1 + s\frac{L}{R}\right)\hat{i}_c(s) + \frac{D}{R}\hat{v}(s) - \frac{D^2}{R}\hat{v}_g(s) \tag{12.56}$$

The equivalent circuit of Fig. 12.21 is now obtained. It can be verified that this equivalent circuit coincides with the model of Fig. 12.15 and the buck converter parameters of Table 12.1.

The approximate small-signal properties of the current programmed buck converter can now be explained. Since the inductor is in series with the current source $\hat{i}_c$, the inductor does not contribute to the control-to-output transfer function. The control-to-output transfer function is determined simply by the relation

$$G_{vc}(s) = \left.\frac{\hat{v}(s)}{\hat{i}_c(s)}\right|_{\hat{v}_g = 0} = \left(R \parallel \frac{1}{sC}\right) \tag{12.57}$$

So current programming transforms the output characteristic of the buck converter into a current source. The power sink input characteristic of the current programmed buck converter leads to a negative incremental input resistance, as described above. Finally, Fig. 12.21 predicts that the buck converter line-to-output transfer function is zero:

$$G_{vg}(s) = \left.\frac{\hat{v}(s)}{\hat{v}_g(s)}\right|_{\hat{i}_c = 0} = 0 \tag{12.58}$$

Disturbances in v_g do not influence the output voltage, since the inductor current depends only on i_c. The current programmed controller adjusts the duty cycle as necessary to maintain constant inductor current, regardless of variations in v_g. The more accurate models of Section 12.3 predict that $G_{vg}(s)$ is not zero, but is nonetheless small in magnitude.

Similar arguments lead to the boost converter small-signal equivalent circuit of Fig. 12.22. Derivation of this equivalent circuit is left as a homework problem. In the case of the boost converter, the switch network input port behaves as a current source, of value i_c, while the output port is a dependent power source, equal to the power apparently consumed by the current source i_c. In the small-signal model, the current source $\hat{i}_c$ appears in series with the inductor L, and hence the converter transfer functions cannot contain poles arising from the inductor. The switch network power source output characteristic leads to an ac resistance of value $r_2 = R$. The line-to-output transfer function $G_{vg}(s)$ is nonzero in the

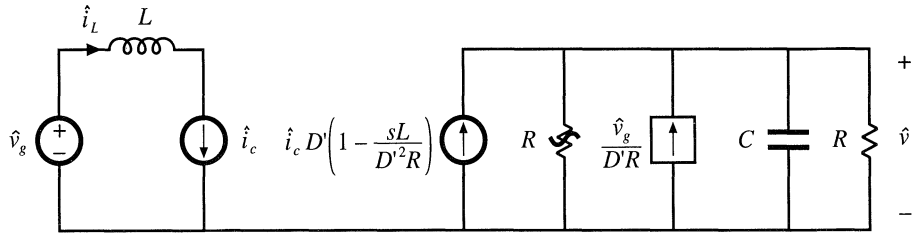

Fig. 12.22 Small-signal model of the CCM CPM boost converter, derived via averaged switch modeling and the approximation $i_L \approx i_c$.

boost converter, since the magnitude of the power source depends directly on the value of v_g. The control-to-output transfer function $G_{vc}(s)$ contains a right half-plane zero, identical to the right half-plane zero of the duty-cycle-controlled boost converter.

12.3 A MORE ACCURATE MODEL

The simple models discussed in the previous section yield much insight into the low-frequency behavior of current-programmed converters. Unfortunately, they do not always describe everything that we need to know. For example, the simple model of the buck converter predicts that the line-to-output transfer function $G_{vg}(s)$ is zero. While it is true that this transfer function is usually small in magnitude, the transfer function is not equal to zero. To predict the effect of input voltage disturbances on the output voltage, we need to compute the actual $G_{vg}(s)$.

In this section, a more accurate analysis is performed which does not rely on the approximation $\langle i_L(t) \rangle_{T_s} \approx i_C(t)$. The analytical approach of [5,6] is combined with the controller model of [7]. A functional block diagram of the current programmed controller is constructed, which accounts for the presence of the artificial ramp and for the inductor current ripple. This block diagram is appended to the averaged converter models derived in Chapter 7, leading to a complete converter CPM model. Models for the CPM buck, boost, and buck–boost converters are listed, and the buck converter model is analyzed in detail.

12.3.1 Current Programmed Controller Model

Rather than using the approximation $\langle i_L(t) \rangle_{T_s} = \langle i_c(t) \rangle_{T_s}$, let us derive a more accurate expression relating the average inductor current $\langle i_L(t) \rangle_{T_s}$ to the control input $i_c(t)$. The inductor current waveform is illustrated in Fig. 12.23. It can be seen that the peak value of $i_L(t)$ differs from $i_c(t)$, by the magnitude of the artificial ramp waveform at time $t = dT_s$, that is, by $m_a dT_s$. The peak and average values of the inductor current waveform differ by the average value of the inductor current ripple. Under transient conditions, in which $i_L(0)$ is not equal to $i_L(T_s)$, the magnitudes of the inductor current ripples during the dT_s and $d'T_s$ subintervals are $m_1 dT_s/2$ and $m_2 d'T_s/2$, respectively. Hence, the average value of the inductor current ripple is $d(m_1 dT_s/2) + d'(m_2 d'T_s/2)$. We can express the average inductor current as

$$\begin{aligned} \langle i_L(t) \rangle_{T_s} &= \langle i_c(t) \rangle_{T_s} - m_a dT_s - d\frac{m_1 dT_s}{2} - d'\frac{m_2 d'T_s}{2} \\ &= \langle i_c(t) \rangle_{T_s} - m_a dT_s - m_1 \frac{d^2 T_s}{2} - m_2 \frac{d'^2 T_s}{2} \end{aligned} \tag{12.59}$$

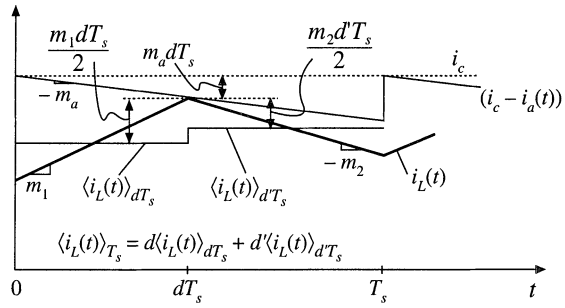

Fig. 12.23 Accurate determination of the relationship between the average inductor current $\langle i_L(t)\rangle_{T_s}$ and i_c.

This is the more accurate relationship which is employed in this section.

A small-signal current programmed controller model is found by perturbation and linearization of Eq. (12.59). Let

$$\begin{aligned}
\langle i_L(t)\rangle_{T_s} &= I_L + \hat{i}_L(t) \\
\langle i_c(t)\rangle_{T_s} &= I_c + \hat{i}_c(t) \\
d(t) &= D + \hat{d}(t) \\
m_1(t) &= M_1 + \hat{m}_1(t) \\
m_2(t) &= M_2 + \hat{m}_2(t)
\end{aligned} \tag{12.60}$$

Note that it is necessary to perturb the slopes m_1 and m_2, since the inductor current slope depends on the converter voltages according to Eq. (12.1). For the basic buck, boost, and buck–boost converters, the slope variations are given by

Buck converter

$$\hat{m}_1 = \frac{\hat{v}_g - \hat{v}}{L} \qquad \hat{m}_2 = \frac{\hat{v}}{L}$$

Boost converter

$$\hat{m}_1 = \frac{\hat{v}_g}{L} \qquad \hat{m}_2 = \frac{\hat{v} - \hat{v}_g}{L} \tag{12.61}$$

Buck–boost converter

$$\hat{m}_1 = \frac{\hat{v}_g}{L} \qquad \hat{m}_2 = -\frac{\hat{v}}{L}$$

It is assumed that m_a does not vary: $\hat{m}_a = M_a$. Substitution of Eq. (12.60) into Eq. (12.59) leads to

$$\left(I_L + \hat{i}_L(t)\right) = \left(I_c + \hat{i}_c(t)\right) - M_a T_s\left(D + \hat{d}(t)\right) - \frac{T_s}{2}\left(M_1 + \hat{m}_1(t)\right)\left(D + \hat{d}(t)\right)^2 - \frac{T_s}{2}\left(M_2 + \hat{m}_2(t)\right)\left(D' - \hat{d}(t)\right)^2 \tag{12.62}$$

The first-order ac terms are

$$\hat{i}_L(t) = \hat{i}_c(t) - \left(M_a T_s + DM_1 T_s - D'M_2 T_s\right)\hat{d}(t) - \frac{D^2 T_s}{2}\hat{m}_1(t) - \frac{D'^2 T_s}{2}\hat{m}_2(t) \tag{12.63}$$

With use of the equilibrium relationship $DM_1 = D'M_2$, Eq. (12.63) can be further simplified:

Table 12.2 Current programmed controller gains for basic converters

Converter	F_g	F_v
Buck	$\frac{D^2T_s}{2L}$	$\frac{(1-2D)T_s}{2L}$
Boost	$\frac{(2D-1)T_s}{2L}$	$\frac{D'^2T_s}{2L}$
Buck–boost	$\frac{D^2T_s}{2L}$	$-\frac{D'^2T_s}{2L}$

$$\hat{i}_L(t) = \hat{i}_c(t) - M_a T_s \hat{d}(t) - \frac{D^2 T_s}{2}\hat{m}_1(t) - \frac{D'^2 T_s}{2}\hat{m}_2(t) \tag{12.64}$$

Finally, solution for $\hat{d}(t)$ yields

$$\hat{d}(t) = \frac{1}{M_a T_s}\left[\hat{i}_c(t) - \hat{i}_L(t) - \frac{D^2 T_s}{2}\hat{m}_1(t) - \frac{D'^2 T_s}{2}\hat{m}_2(t)\right] \tag{12.65}$$

This is the actual relationship that the current programmed controller follows, to determine $\hat{d}(t)$ as a function of $\hat{i}_c(t)$, $\hat{i}_L(t)$, $\hat{m}_1(t)$, and $\hat{m}_2(t)$. Since the quantities $\hat{m}_1(t)$, and $\hat{m}_2(t)$ depend on $\hat{v}_g(t)$ and $\hat{v}(t)$, according to Eq. (12.61), we can express Eq. (12.65) in the following form:

$$\hat{d}(t) = F_m\left[\hat{i}_c(t) - \hat{i}_L(t) - F_g\hat{v}_g(t) - F_v\hat{v}(t)\right] \tag{12.66}$$

where $F_m = 1/M_a T_s$. Expressions for the gains F_g and F_v, for the basic buck, boost, and buck–boost converters, are listed in Table 12.2. A functional block diagram of the current programmed controller, corresponding to Eq. (12.66), is constructed in Fig. 12.24.

Current programmed converter models can now be obtained, by combining the controller block

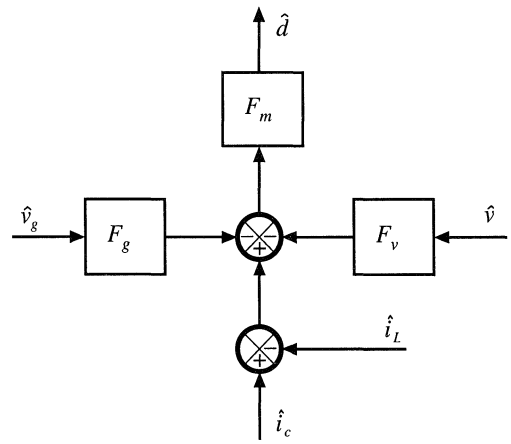

Fig. 12.24 Functional block diagram of the current programmed controller.

diagram of Fig. 12.24 with the averaged converter models derived in Chapter 7. Figure 12.25 illustrates the CPM converter models obtained by combination of Fig. 12.24 with the buck, boost, and buck-boost models of Fig. 7.17. For each converter, the current programmed controller contains effective feedback of the inductor current $\hat{i}_L(t)$ and the output voltage $\hat{v}(t)$, as well as effective feedforward of the input voltage $\hat{v}_g(t)$.

12.3.2 Solution of the CPM Transfer Functions

Next, let us solve the models of Fig. 12.25, to determine more accurate expressions for the control-to-output and line-to-output transfer functions of current-programmed buck, boost, and buck–boost converters. As discussed in Chapter 8, the converter output voltage $\hat{v}$ can be expressed as a function of the duty-cycle $\hat{d}$ and input voltage $\hat{v}_g$ variations, using the transfer functions $G_{vd}(s)$ and $G_{vg}(s)$:

$$\hat{v}(s) = G_{vd}(s)\hat{d}(s) + G_{vg}(s)\hat{v}_g(s) \tag{12.67}$$

In a similar manner, the inductor current variation $\hat{i}$ can be expressed as a function of the duty-cycle $\hat{d}$ and input voltage $\hat{v}_g$ variations, by defining the transfer functions $G_{id}(s)$ and $G_{ig}(s)$:

$$\hat{i}_L(s) = G_{id}(s)\hat{d}(s) + G_{ig}(s)\hat{v}_g(s) \tag{12.68}$$

where the transfer functions $G_{id}(s)$ and $G_{ig}(s)$ are given by:

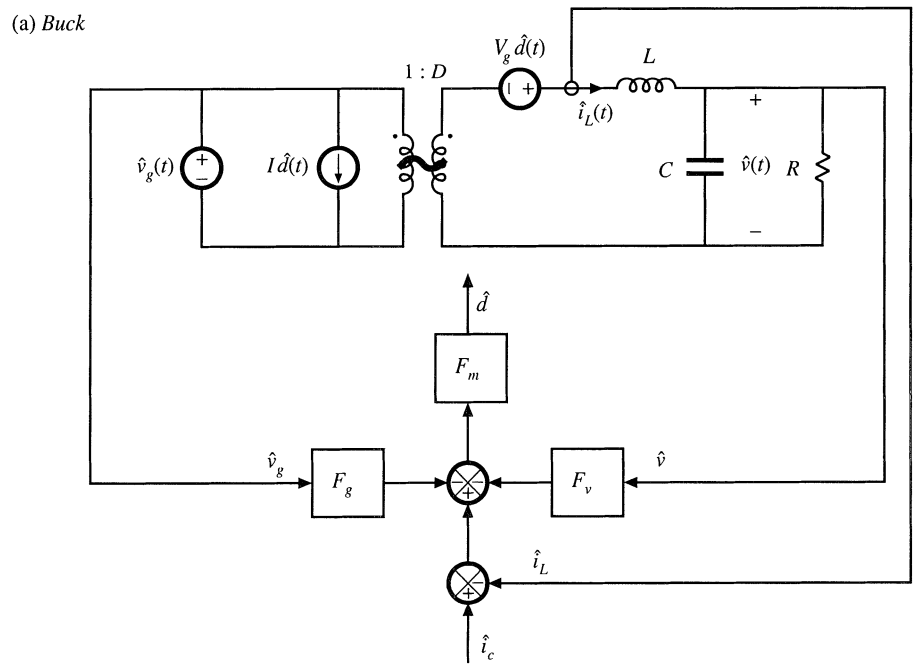

Fig. 12.25 More accurate models of current-programmed converters: (a) buck, (b) boost, (c) buck–boost.

(b) *Boost*

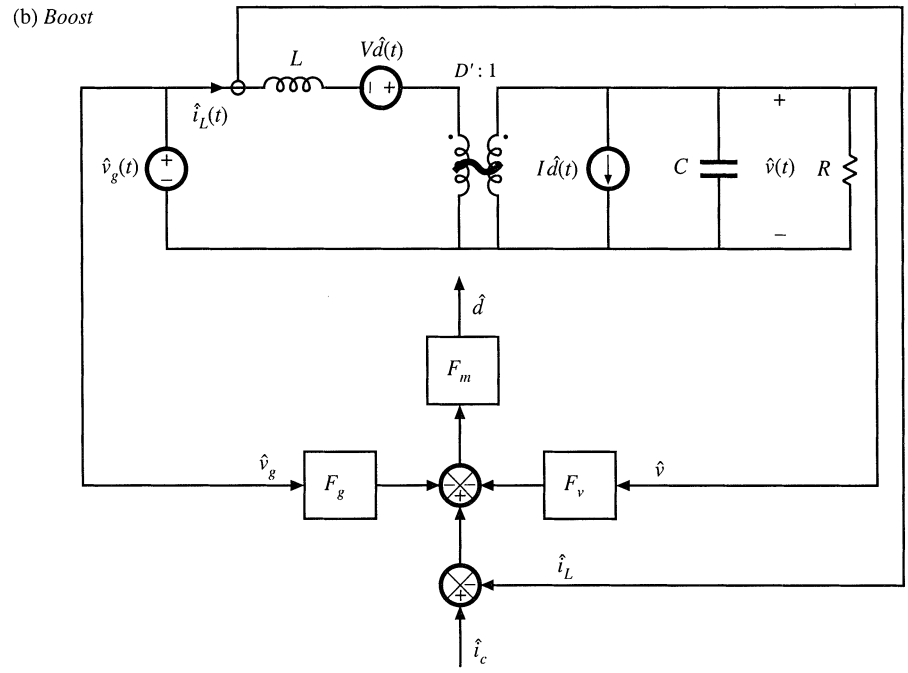

(c) *Buck–boost*

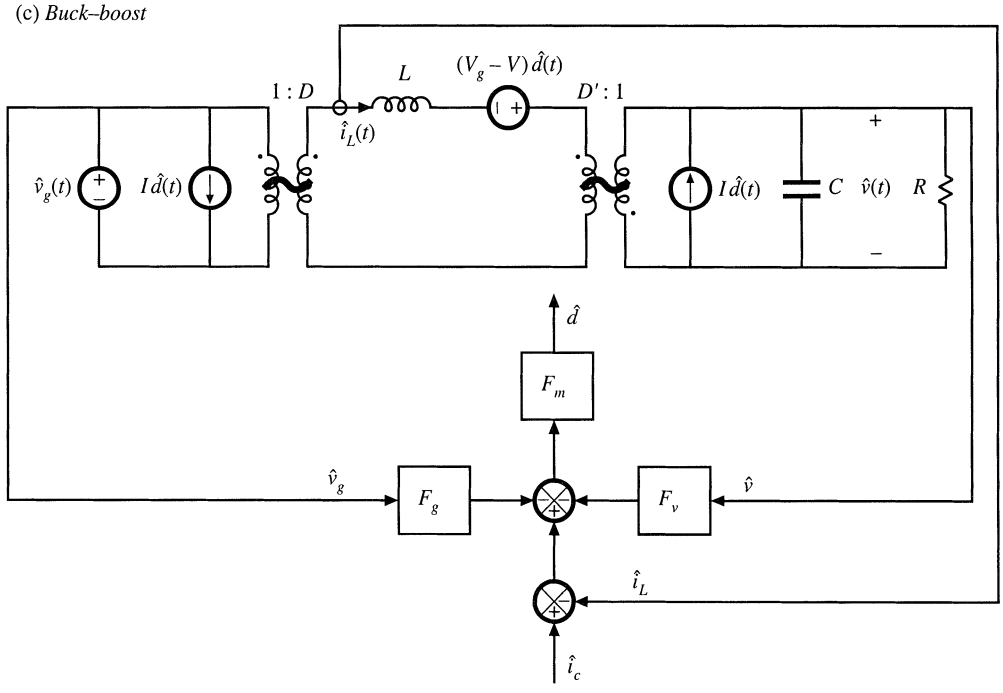

Fig. 12.25 Continued.

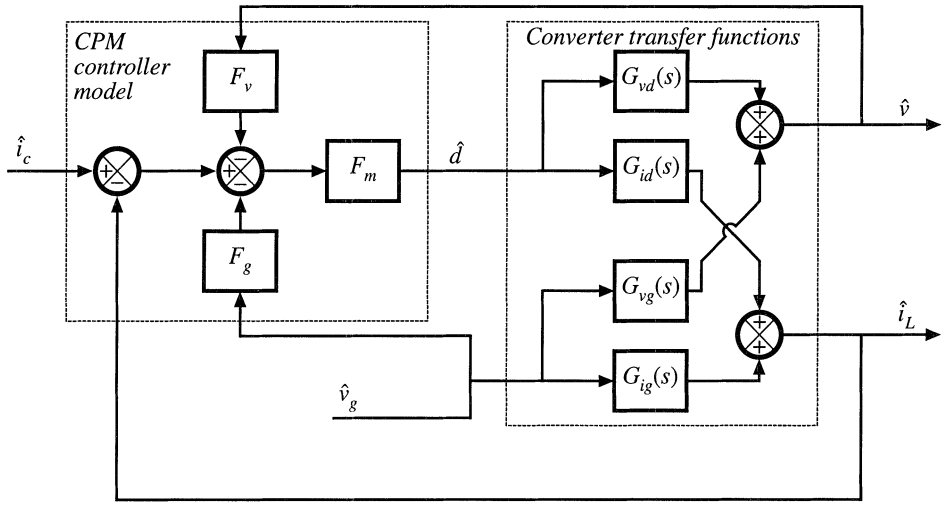

Fig. 12.26 Block diagram that models the current-programmed converters of Fig. 12.25.

$$G_{id}(s) = \left.\frac{\hat{i}_L(s)}{\hat{d}(s)}\right|_{\hat{v}_g(s)=0}$$
$$G_{ig}(s) = \left.\frac{\hat{i}_L(s)}{\hat{v}_g(s)}\right|_{\hat{d}(s)=0} \tag{12.69}$$

Figure 12.26 illustrates replacement of the converter circuit models of Fig. 12.25 with block diagrams that correspond to Eqs. (12.67) and (12.68).

The control-to-output and line-to-output transfer functions can now be found, by manipulation of the block diagram of Fig. 12.26, or by algebraic elimination of $\hat{d}$ and $\hat{i}_L$ from Eqs. (12.66), (12.67), and (12.68), and solution for $\hat{v}$. Substitution of Eq. (12.68) into Eq. (12.66) and solution for $\hat{d}$ leads to

$$\hat{d} = \frac{F_m}{\left(1 + F_m G_{id}\right)}\left[\hat{i}_c - \left(G_{ig} + F_g\right)\hat{v}_g - F_v\hat{v}\right] \tag{12.70}$$

By substituting this expression into Eq. (12.67), one obtains

$$\hat{v} = \frac{F_m G_{vd}}{\left(1 + F_m G_{id}\right)}\left[\hat{i}_c - \left(G_{ig} + F_g\right)\hat{v}_g - F_v\hat{v}\right] + G_{vg}\hat{v}_g \tag{12.71}$$

Solution of this equation for $\hat{v}$ leads to the desired result:

$$\hat{v} = \frac{F_m G_{vd}}{1 + F_m\left(G_{id} + F_v G_{vd}\right)}\hat{i}_c + \frac{G_{vg} - F_m F_g G_{vd} + F_m\left(G_{vg}G_{id} - G_{ig}G_{vd}\right)}{1 + F_m\left(G_{id} + F_v G_{vd}\right)}\hat{v}_g \tag{12.72}$$

Therefore, the current-programmed control-to-output transfer function is

$$G_{vc}(s) = \left.\frac{\hat{v}(s)}{\hat{i}_c(s)}\right|_{\hat{v}_g(s)=0} = \frac{F_m G_{vd}}{1 + F_m\left(G_{id} + F_v G_{vd}\right)} \tag{12.73}$$

The current-programmed line-to-output transfer function is

$$G_{vg\text{-}cpm}(s) = \left.\frac{\hat{v}(s)}{\hat{v}_g(s)}\right|_{\hat{i}_c(s)=0} = \frac{G_{vg} - F_m F_g G_{vd} + F_m\left(G_{vg}G_{id} - G_{ig}G_{vd}\right)}{1 + F_m\left(G_{id} + F_v G_{vd}\right)} \tag{12.74}$$

Equations (12.73) and (12.74) are general expressions for the important transfer functions of single-inductor current-programmed converters operating in the continuous conduction mode.

12.3.3 Discussion

The controller model of Eq. (12.66) and Fig. 12.24 accounts for the differences between i_L and i_c that arise by two mechanisms: the inductor current ripple and the artificial ramp. The inductor current ripple causes the peak and average values of the inductor current to differ; this leads to a deviation between the average inductor current and i_c. Since the magnitude of the inductor current ripple is a function of the converter input and capacitor voltages, this mechanism introduces $\hat{v}_g$ and $\hat{v}$ dependencies into the controller small-signal block diagram. Thus, the F_g and F_v gain blocks of Fig. 12.24 model the small-signal effects of the inductor current ripple. For operation deep in continuous conduction mode ($2L/RT_s \gg 1$), the inductor current ripple is small. The F_g and F_v gain blocks can then be ignored, and the inductor current ripple has negligible effect on the current programmed controller gain.

The artificial ramp also causes the average inductor current to differ from i_c. This is modeled by the gain block F_m, which depends inversely on the artificial ramp slope M_a. With no artificial ramp, $M_a = 0$ and F_m tends to infinity. The current-programmed control systems of Fig. 12.25 then effectively have infinite loop gain. Since the duty cycle $\hat{d}$ is finite, the signal at the input to the F_m block ($\hat{d}/F_m$) must tend to zero. The block diagram then predicts that

$$\frac{\hat{d}}{F_m} = 0 = \hat{i}_c - \hat{i}_L - F_g\hat{v}_g - F_v\hat{v} \tag{12.75}$$

In the case of negligible inductor current ripple ($F_g \to 0$ and $F_v \to 0$), this equation further reduces to

$$0 = \hat{i}_c - \hat{i}_L \tag{12.76}$$

This coincides with the simple approximation employed in Section 12.2. Hence, the transfer functions predicted in this section reduce to the results of Section 12.2 when there is no artificial ramp and negligible inductor current ripple. In the limit when $F_m \to \infty$, $F_g \to 0$, and $F_v \to 0$, the control-to-output transfer function (12.73) reduces to

$$\lim_{\substack{F_m \to \infty \\ F_g \to 0 \\ F_v \to 0}} G_{vc}(s) = \frac{G_{vd}}{G_{id}} \tag{12.77}$$

and the line-to-output transfer function reduces to

$$\lim_{\substack{F_m \to \infty \\ F_g \to 0 \\ F_v \to 0}} G_{vg\text{-}cpm}(s) = \frac{G_{vg}G_{id} - G_{ig}G_{vd}}{G_{id}} \tag{12.78}$$

It can be verified that Eqs. (12.77) and (12.78) are equivalent to the transfer functions derived in Section 12.2.

When an artificial ramp is present, then the gain F_m is reduced to a finite value. The current-programmed controller no longer perfectly regulates the inductor current i_L, and the terms on the right-hand side of Eq. (12.75) do not add to zero. In the extreme case of a very large artificial ramp (large M_a and hence small F_m), the current-programmed controller degenerates to duty-cycle control. The artificial ramp and analog comparator of Fig. 12.8 then function as a pulse-width modulator similar to Fig. 7.63, with small-signal gain F_m. For small F_m and for $F_g \to 0$, $F_v \to 0$, the control-to-output transfer function (12.73) reduces to

$$\lim_{\substack{\text{small } F_m \\ F_v \to 0 \\ F_g \to 0}} G_{vc}(s) = F_m G_{vd}(s) \tag{12.79}$$

which coincides with conventional duty cycle control. Likewise, Eq. (12.74) reduces to

$$\lim_{\substack{F_m \to \infty \\ F_g \to 0 \\ F_v \to 0}} G_{vg\text{-}cpm}(s) = G_{vg} \tag{12.80}$$

which is the line-to-output transfer function for conventional duty cycle control.

12.3.4 Current-Programmed Transfer Functions of the CCM Buck Converter

The control-to-output transfer function $G_{vd}(s)$ and line-to-output transfer function $G_{vg}(s)$ of the CCM buck converter with duty cycle control are tabulated in Chapter 8, by analysis of the equivalent circuit model in Fig. 7.17(a). The results are:

$$G_{vd}(s) = \frac{V}{D} \frac{1}{den(s)} \tag{12.81}$$

$$G_{vg}(s) = D \frac{1}{den(s)} \tag{12.82}$$

where the denominator polynomial is

$$den(s) = 1 + s\frac{L}{R} + s^2 LC \tag{12.83}$$

The inductor current transfer functions $G_{id}(s)$ and $G_{ig}(s)$ defined by Eqs. (12.68) and (12.69) are also found by solution of the equivalent circuit model in Fig. 7.17(a), with the following results:

$$G_{id}(s) = \frac{V}{DR} \frac{\left(1 + sRC\right)}{den(s)} \tag{12.84}$$

$$G_{ig}(s) = \frac{D}{R}\frac{\left(1 + sRC\right)}{den(s)} \tag{12.85}$$

where $den(s)$ is again given by Eq. (12.83).

With no artificial ramp and negligible ripple, the control-to-output transfer function reduces to the ideal expression (12.77). Substitution of Eqs. (12.81) and (12.84) yields

$$\lim_{\substack{F_m \to \infty \\ F_g \to 0 \\ F_v \to 0}} G_{vc}(s) = \frac{G_{vd}(s)}{G_{id}(s)} = \frac{R}{1 + sRC} \tag{12.86}$$

Under the same conditions, the line-to-output transfer function reduces to the ideal expression (12.78). Substitution of Eqs. (12.81) to (12.85) leads to

$$\lim_{\substack{F_m \to \infty \\ F_g \to 0 \\ F_v \to 0}} G_{vg\text{-}cpm}(s) = \frac{G_{vg}(s)G_{id}(s) - G_{vd}(s)G_{ig}(s)}{G_{id}(s)} = 0 \tag{12.87}$$

Equations (12.86) and (12.87) coincide with the expressions derived in Section 12.2 for the CCM buck converter.

For arbitrary F_m, F_v, and F_g, the control-to-output transfer function is given by Eq. (12.73). Substitution of Eqs. (12.81) to (12.85) into Eq. (12.73) yields

$$G_{vc}(s) = \frac{F_m G_{vd}}{1 + F_m\left[G_{id} + F_v G_{vd}\right]} = \frac{F_m\left(\frac{V}{D}\frac{1}{den(s)}\right)}{1 + F_m\left[\left(\frac{V}{DR}\frac{1 + sRC}{den(s)}\right) + F_v\left(\frac{V}{D}\frac{1}{den(s)}\right)\right]} \tag{12.88}$$

Simplification leads to

$$G_{vc}(s) = \frac{F_m\frac{V}{D}}{den(s) + \frac{F_m V}{DR}\left(1 + sRC\right) + F_m F_v\frac{V}{D}} \tag{12.89}$$

Finally, the control-to-output transfer function can be written in the following normalized form:

$$G_{vc}(s) = \frac{G_{c0}}{1 + \frac{s}{Q_c\omega_c} + \left(\frac{s}{\omega_c}\right)^2} \tag{12.90}$$

where

$$G_{c0} = \frac{V}{D}\frac{F_m}{1 + \frac{F_m V}{DR} + \frac{F_m F_v V}{D}} \tag{12.91}$$

$$\omega_c = \frac{1}{\sqrt{LC}}\sqrt{1 + \frac{F_m V}{DR} + \frac{F_m F_v V}{D}} \tag{12.92}$$

$$Q_c = R\sqrt{\frac{C}{L}}\,\frac{\sqrt{1+\dfrac{F_m V}{DR}+\dfrac{F_m F_v V}{D}}}{\left(1+\dfrac{RCF_m V}{DL}\right)} \tag{12.93}$$

In the above equations, the salient features G_{c0}, ω_c, and Q_c are expressed as the duty-ratio-control value, multiplied by a factor that accounts for the effects of current-programmed control.

It can be seen from Eq. (12.93) that current programming tends to reduce the Q-factor of the poles. For large F_m, Q_c varies as $F_m^{-1/2}$; consequently, the poles become real and well-separated in magnitude. The low-Q approximation of Section 8.1.7 then predicts that the low-frequency pole becomes

$$Q_c\omega_c = \frac{R}{L}\,\frac{\left(1+\dfrac{F_m V}{DR}+\dfrac{F_m F_v V}{D}\right)}{\left(1+\dfrac{RCF_m V}{DL}\right)} \tag{12.94}$$

For large F_m and small F_v, this expression can be further approximated as

$$Q_c\omega_c \approx \frac{1}{RC} \tag{12.95}$$

which coincides with the low-frequency pole predicted by the simple model of Section 12.2. The low-Q approximation also predicts that the high-frequency pole becomes

$$\frac{\omega_c}{Q_c} = \frac{1}{RC}\left(1+\frac{RCF_m V}{DL}\right) \tag{12.96}$$

For large F_m, this expression can be further approximated as

$$\frac{\omega_c}{Q_c} \approx \frac{F_m V}{DL} = f_s\frac{M_2}{DM_a} \tag{12.97}$$

The high-frequency pole is typically predicted to lie near to or greater than the switching frequency f_s. It should be pointed out that the converter switching and modulator sampling processes lead to discrete-time phenomena that affect the high-frequency behavior of the converter, and that are not predicted by the continuous-time averaged analysis employed here. Hence, the averaged model is valid only at frequencies sufficiently less than one-half of the switching frequency.

For arbitrary F_m, F_v, and F_g, the current-programmed line-to-output transfer function $G_{vg\text{-}cpm}(s)$ is given by Eq. (12.74). This equation is most easily evaluated by first finding the ideal transfer function, Eq. (12.78), and then using the result to simplify Eq. (12.74). In the case of the buck converter, Eq. (12.87) shows that the quantity $(G_{vg}G_{id} - G_{vd}G_{ig})$ is equal to zero. Hence, Eq. (12.74) becomes

$$G_{vg\text{-}cpm}(s) = \frac{G_{vg} - F_m F_g G_{vd} + F_m(0)}{1 + F_m\left(G_{id} + F_v G_{vd}\right)} \tag{12.98}$$

Substitution of Eqs. (12.81) to (12.85) into Eq. (12.98) yields

$$G_{vg\text{-}cpm}(s) = \frac{\frac{D}{den(s)} - F_m F_g \frac{V}{D}\frac{1}{den(s)}}{1 + F_m\left(\frac{V}{DR}\frac{1+sRC}{den(s)} + F_v\frac{V}{D}\frac{1}{den(s)}\right)} \tag{12.99}$$

Simplification leads to

$$G_{vg\text{-}cpm}(s) = \frac{\left(D - F_m F_g \frac{V}{D}\right)}{den(s) + \frac{F_m V}{DR}\left(1+sRC\right) + F_m F_v \frac{V}{D}} \tag{12.100}$$

Finally, the current-programmed line-to-output transfer function can be written in the following normalized form:

$$G_{vg\text{-}cpm}(s) = \frac{G_{g0}}{1 + \frac{s}{Q_c\omega_c} + \left(\frac{s}{\omega_c}\right)^2} \tag{12.101}$$

where

$$G_{g0} = D\frac{\left(1 - \frac{F_m F_g V}{D^2}\right)}{\left(1 + \frac{F_m V}{DR} + \frac{F_m F_v V}{D}\right)} = D\frac{\left(1 - \frac{M_2}{2M_a}\right)}{\left(1 + \frac{F_m V}{DR} + \frac{F_m F_v V}{D}\right)} \tag{12.102}$$

The quantities Q_c and ω_c are given by Eqs. (12.92) and (12.93).

Equation (12.102) shows how current programming reduces the dc gain of the buck converter line-to-output transfer function. For duty cycle control ($F_m \to 0$), G_{g0} is equal to D. Nonzero values of F_m reduce the numerator and increase the denominator of Eq. (12.102), which tends to reduce G_{g0}. We have already seen that, in the ideal case ($F_m \to \infty$, $F_g \to 0$, $F_v \to 0$), G_{g0} becomes zero. Equation (12.102) reveals that nonideal current-programmed buck converters can also exhibit zero G_{g0}, if the artificial ramp slope M_a is chosen equal to $0.5M_2$. The current programmed controller then prevents input line voltage variations from reaching the output. The mechanism that leads to this result is the effective feedforward of v_g, inherent in the current programmed controller via the $F_g\hat{v}_g$ term in Eq. (12.66). It can be seen from Fig. 12.26 that, when $F_g F_m G_{vd}(s) = G_{vg}(s)$, then the feedforward path from $\hat{v}_g$ through F_g induces variations in the output $\hat{v}$ that exactly cancel the $\hat{v}_g$-induced variations in the direct forward path of the converter through $G_{vg}(s)$. This cancellation occurs in the buck converter when $M_a = 0.5M_2$.

12.3.5 Results for Basic Converters

The transfer functions of the basic buck, boost, and buck-boost converters with current-programmed control are summarized in Tables 12.3 to 12.5. Control-to-output and line-to-output transfer functions for both the simple model of Section 12.2 and the more accurate model derived in this section are listed. For completeness, the transfer functions for duty cycle control are included. In each case, the salient features are expressed as the corresponding quantity with duty cycle control, multiplied by a factor that accounts for current-programmed control.

Table 12.3 Summary of results for the CPM buck converter

Simple model

$$\frac{\hat{v}}{\hat{i}_c} = \frac{R}{1 + sRC}$$

$$\frac{\hat{v}}{\hat{v}_g} = 0$$

Duty cycle controlled gains

$$G_{vd}(s) = \frac{V}{D}\frac{1}{den(s)} \qquad G_{id}(s) = \frac{V}{DR}\frac{1 + sRC}{den(s)}$$

$$G_{vg}(s) = D\frac{1}{den(s)} \qquad G_{ig}(s) = \frac{D}{R}\frac{1 + sRC}{den(s)}$$

$$den(s) = 1 + s\frac{L}{R} + s^2LC$$

More accurate model

$$\frac{\hat{v}}{\hat{i}_c} = G_{vc}(s) = G_{c0}\frac{1}{1 + \frac{s}{Q_c\omega_c} + \left(\frac{s}{\omega_c}\right)^2}$$

$$G_{c0} = \frac{V}{D}\frac{F_m}{\left(1 + \frac{F_mV}{DR} + \frac{F_mF_vV}{D}\right)}$$

$$\omega_c = \frac{1}{\sqrt{LC}}\sqrt{1 + \frac{F_mV}{DR} + \frac{F_mF_vV}{D}}$$

$$Q_c = R\sqrt{\frac{C}{L}}\frac{\sqrt{1 + \frac{F_mV}{DR} + \frac{F_mF_vV}{D}}}{\left(1 + \frac{RCF_mV}{DL}\right)}$$

$$\frac{\hat{v}}{\hat{v}_g} = G_{vg\text{-}cpm}(s) = G_{g0}\frac{1}{1 + \frac{s}{Q_c\omega_c} + \left(\frac{s}{\omega_c}\right)^2}$$

$$G_{g0} = D\frac{\left(1 - \frac{F_mF_gV}{D^2}\right)}{\left(1 + \frac{F_mV}{DR} + \frac{F_mF_vV}{D}\right)}$$

Table 12.4 Summary of results for the CPM boost converter

Simple model

$$\frac{\hat{v}}{\hat{i}_c} = \frac{D'R}{2}\frac{\left(1 - s\frac{L}{D'^2R}\right)}{\left(1 + s\frac{RC}{2}\right)}$$

$$\frac{\hat{v}}{\hat{v}_g} = \frac{1}{2D'}\frac{1}{\left(1 + s\frac{RC}{2}\right)}$$

Duty cycle controlled gains

$$G_{vd}(s) = \frac{V}{D'}\frac{\left(1 - s\frac{L}{D'^2R}\right)}{den(s)} \qquad G_{id}(s) = \frac{2V}{D'^2R}\frac{\left(1 + s\frac{RC}{2}\right)}{den(s)}$$

$$G_{vg}(s) = \frac{1}{D'}\frac{1}{den(s)} \qquad G_{ig}(s) = \frac{1}{D'^2R}\frac{\left(1 + sRC\right)}{den(s)}$$

$$den(s) = 1 + s\frac{L}{D'^2R} + s^2\frac{LC}{D'^2}$$

More accurate model

$$\frac{\hat{v}}{\hat{i}_c} = G_{vc}(s) = G_{c0}\frac{\left(1 - s\frac{L}{D'^2R}\right)}{1 + \frac{s}{Q_c\omega_c} + \left(\frac{s}{\omega_c}\right)^2}$$

$$G_{c0} = \frac{V}{D'}\frac{F_m}{\left(1 + \frac{2F_mV}{D'^2R} + \frac{F_mF_vV}{D'}\right)}$$

$$\omega_c = \frac{D'}{\sqrt{LC}}\sqrt{1 + \frac{2F_mV}{D'^2R} + \frac{F_mF_vV}{D'}}$$

$$Q_c = D'R\sqrt{\frac{C}{L}}\frac{\sqrt{1 + \frac{2F_mV}{D'^2R} + \frac{F_mF_vV}{D'}}}{\left(1 + RC\frac{F_mV}{L} - \frac{F_mF_vV}{D'}\right)}$$

$$\frac{\hat{v}}{\hat{v}_g} = G_{vg\text{-}cpm}(s) = G_{g0}\frac{\left(1 + \frac{s}{\omega_{gz}}\right)}{1 + \frac{s}{Q_c\omega_c} + \left(\frac{s}{\omega_c}\right)^2}$$

$$G_{g0} = \frac{1}{D'}\frac{\left(1 - F_mF_gV + \frac{F_mV}{D'^2R}\right)}{\left(1 + \frac{2F_mV}{D'^2R} + \frac{F_mF_vV}{D'}\right)}$$

$$\omega_{gz} = \frac{D'^3R}{L}\frac{\left(1 - F_mF_gV + \frac{F_mV}{D'^2R}\right)}{F_mF_gV}$$

Table 12.5 Summary of results for the CPM buck–boost converter

Simple model

$$\frac{\hat{v}}{\hat{i}_c} = -\frac{D'R}{(1+D)} \frac{\left(1 - s\frac{DL}{D'^2R}\right)}{\left(1 + s\frac{RC}{1+D}\right)}$$

$$\frac{\hat{v}}{\hat{v}_g} = -\frac{D^2}{1-D^2} \frac{1}{\left(1 + s\frac{RC}{1+D}\right)}$$

Duty cycle controlled gains

$$G_{vd}(s) = -\frac{|V|}{DD'} \frac{\left(1 - s\frac{DL}{D'^2R}\right)}{den(s)}$$

$$G_{vg}(s) = -\frac{D}{D'} \frac{1}{den(s)}$$

$$G_{id}(s) = -\frac{|V|(1+D)}{DD'^2R} \frac{\left(1 + s\frac{RC}{(1+D)}\right)}{den(s)}$$

$$G_{ig}(s) = \frac{D}{D'^2R} \frac{\left(1 + sRC\right)}{den(s)}$$

$$den(s) = 1 + s\frac{L}{D'^2R} + s^2\frac{LC}{D'^2}$$

More accurate model

$$\frac{\hat{v}}{\hat{i}_c} = G_{vc}(s) = G_{c0} \frac{\left(1 - s\frac{DL}{D'^2R}\right)}{1 + \frac{s}{Q_c\omega_c} + \left(\frac{s}{\omega_c}\right)^2}$$

$$\omega_c = \frac{D'}{\sqrt{LC}} \sqrt{1 + \frac{F_m|V|(1+D)}{DD'^2R} - \frac{F_mF_v|V|}{DD'}}$$

$$\frac{\hat{v}}{\hat{v}_g} = G_{vg\text{-}cpm}(s) = G_{g0} \frac{\left(1 + \frac{s}{\omega_{gz}}\right)}{1 + \frac{s}{Q_c\omega_c} + \left(\frac{s}{\omega_c}\right)^2}$$

$$G_{c0} = -\frac{|V|}{DD'} \frac{F_m}{\left(1 + \frac{F_m|V|(1+D)}{DD'^2R} - \frac{F_mF_v|V|}{DD'}\right)}$$

$$Q_c = D'R\sqrt{\frac{C}{L}} \frac{\sqrt{1 + \frac{F_m|V|(1+D)}{DD'^2R} - \frac{F_mF_v|V|}{DD'}}}{\left(1 + \frac{F_m|V|RC}{DL} + \frac{F_mF_v|V|}{D'}\right)}$$

$$G_{g0} = -\frac{D}{D'}\left(1 + \frac{F_m|V|}{D'^2R} - \frac{F_mF_g|V|}{D^2}\right)$$

$$\omega_{gz} = \frac{DD'^2R}{|V|LF_mF_g}\left(1 + \frac{F_m|V|}{D'^2R} - \frac{F_mF_g|V|}{D^2}\right)$$

The two poles of the line-to-output transfer functions $G_{vg\text{-}cpm}$ and control-to-output transfer functions G_{vc} of all three converters typically exhibit low Q-factors in CPM. The low-Q approximation can be applied, as in Eqs. (12.94) to (12.97), to find the low-frequency pole. The line-to-output transfer functions of the boost and buck–boost converters exhibit two poles and one zero, with substantial dc gain.

12.3.6 Quantitative Effects of Current-Programmed Control on the Converter Transfer Functions

The frequency responses of a CCM buck converter, operating with current-programmed control and with duty cycle control, are compared in Appendix B, Section B.3.2. The buck converter of Fig. B.25 was simulated as described in Appendix B, and the resulting plots are reproduced here.

The magnitude and phase of the control-to-output transfer functions are illustrated in Fig. 12.27. It can be seen that, for duty cycle control, the transfer function $G_{vd}(s)$ exhibits a resonant two-pole response. The substantial damping introduced by current-programmed control leads to essentially a single-pole response in the current-programmed control-to-output transfer function $G_{vc}(s)$. A second pole appears in the vicinity of 100 kHz, which is near the 200 kHz switching frequency. Because of this effective single-pole response, it is relatively easy to design a controller that exhibits a well-behaved response,

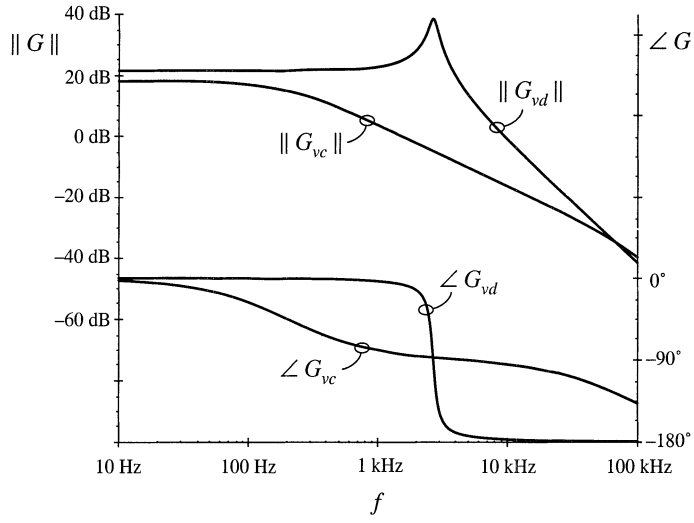

Fig. 12.27 Comparison of CPM control with duty-cycle control, for the control-to-output frequency response of the buck converter example.

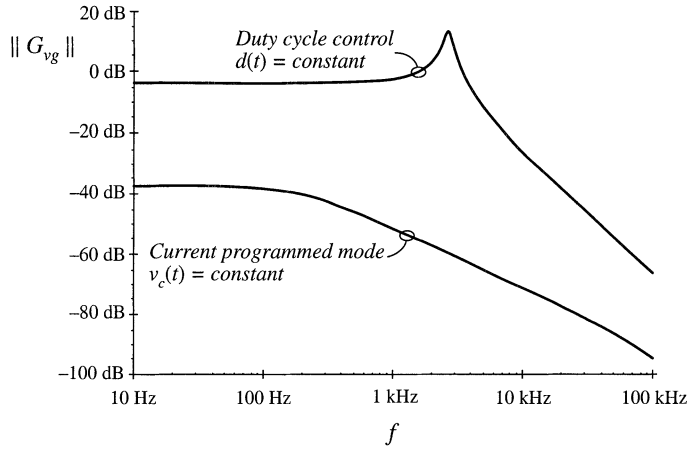

Fig. 12.28 Comparison of CPM control with duty-cycle control, for the line-to-output frequency response of the buck converter example.

having ample phase margin over a wide range of operating points. Proportional-plus-integral (*PI*) controllers are commonly used in current-programmed regulators.

The line-to-output transfer functions of the same example are compared in Fig. 12.28. The line-to-output transfer function $G_{vg}(s)$ for duty-cycle control is characterized by a dc asymptote approximately equal to the duty cycle $D = 0.676$. Resonant poles occur at the corner frequency of the *L–C* filter. The line-to-output transfer function $G_{vg\text{-}cpm}(s)$ with current-programmed control is significantly reduced, and exhibits more than 30 dB of additional attenuation over the frequencies of interest. It should again be

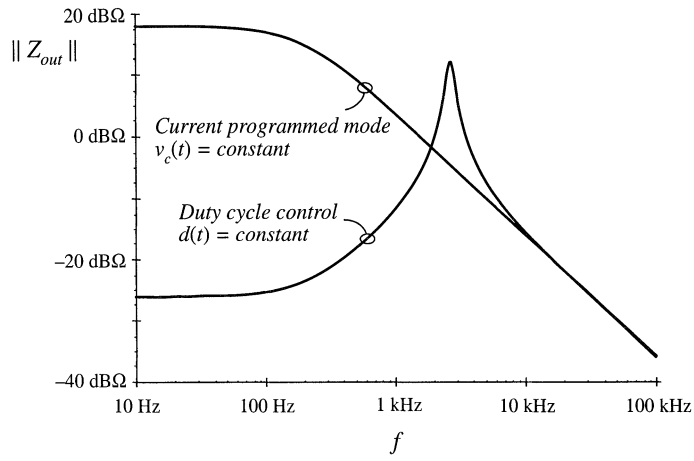

Fig. 12.29 Comparison of CPM control with duty-cycle control, for the output impedance of the buck converter example.

noted that the transfer function $G_{vg\text{-}cpm}(s)$ in Fig. 12.28 cannot be predicted by the simple models of Section 12.2; the more accurate model of Section 12.3 must be employed.

The effect of current-programmed control on the converter output impedance is illustrated in Fig. 12.29. The output impedance plotted in the figure includes the load resistance of 10 Ω. For duty-cycle control, the dc asymptote of the output impedance is dominated by the inductor winding resistance of 0.05 Ω. The inductor becomes significant in the vicinity of 200 Hz. Above the resonant frequency of the output filter, the output impedance is dominated by the output filter capacitor. For current-programmed control, the simple model of Section 12.2 predicts that the inductor branch of the circuit is driven by a current source; this effectively removes the influence of the inductor on the output impedance. The plot of Fig. 12.29 was generated using the more accurate model of this section; nonetheless, the output impedance is accurately predicted by the simple model. The dc asymptote is dominated by the load resistance, and the high-frequency asymptote follows the impedance of the output filter capacitor. It can be seen that current programming substantially increases the converter output impedance.

12.4 DISCONTINUOUS CONDUCTION MODE

Current-programmed converters operating in the discontinuous conduction mode can be described using the averaged switch modeling approaches of Sections 12.3 and 11.1. It is found in this section that the average transistor voltage and current follow a power sink characteristic, while the average diode voltage and current obey a power source characteristic. Perturbation and linearization of these characteristics leads to a small-signal equivalent circuit that models CPM DCM converters. The basic DCM CPM buck, boost, and buck–boost converters essentially exhibit single-pole transfer functions: the second pole and the right half-plane zero appear at frequencies near to or greater than the switching frequency, owing to the small value of L in DCM.

A DCM CPM buck–boost converter example is analyzed here. However, Eqs. (12.103) to (12.120) are written in general form, and apply equally well to DCM CPM buck and boost converters. The schematic of a buck-boost converter is illustrated in Fig. 12.30. The terminal waveforms of the switch network are defined as shown: $v_1(t)$ and $i_1(t)$ are the transistor waveforms, while $v_2(t)$ and $i_2(t)$ are

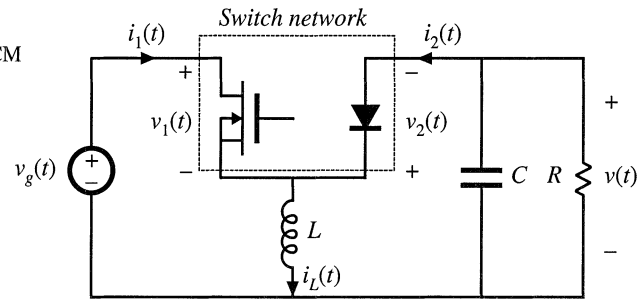

Fig. 12.30 Current-programmed DCM buck–boost converter example.

the diode waveforms. Figure 12.31 illustrates typical DCM waveforms, for current-programmed control with an artificial ramp having slope $-m_a$. The inductor current is zero at the beginning of each switching period. By solution of the transistor conduction subinterval, the programmed current i_{pk} can be related to the transistor duty cycle d_1 by:

$$\begin{aligned} i_c &= i_{pk} + m_a d_1 T_s \\ &= \left(m_1 + m_a\right) d_1 T_s \end{aligned} \tag{12.103}$$

Solution for d_1 leads to

$$d_1(t) = \frac{i_c(t)}{\left(m_1 + m_a\right) T_s} \tag{12.104}$$

The average transistor current is found by integrating the $i_1(t)$ waveform of Fig. 12.31 over one switching period:

$$\left\langle i_1(t) \right\rangle_{T_s} = \frac{1}{T_s} \int_t^{t+T_s} i_1(\tau) d\tau = \frac{q_1}{T_s} \tag{12.105}$$

The total area q_1 is equal to one-half of the peak current i_{pk}, multiplied by the subinterval length $d_1 T_s$. Hence,

$$\left\langle i_1(t) \right\rangle_{T_s} = \tfrac{1}{2} i_{pk}(t) d_1(t) \tag{12.106}$$

Elimination of i_{pk} and d_1, to express the average transistor current as a function of i_c, leads to

$$\left\langle i_1(t) \right\rangle_{T_s} = \frac{\tfrac{1}{2} L i_c^2 f_s}{\left\langle v_1(t) \right\rangle_{T_s} \left(1 + \dfrac{m_a}{m_1}\right)^2} \tag{12.107}$$

Finally, Eq. (12.107) can be rearranged to obtain the averaged switch network input port relationship:

$$\left\langle i_1(t) \right\rangle_{T_s} \left\langle v_1(t) \right\rangle_{T_s} = \frac{\tfrac{1}{2} L i_c^2 f_s}{\left(1 + \dfrac{m_a}{m_1}\right)^2} = \left\langle p(t) \right\rangle_{T_s} \tag{12.108}$$

Thus, the average transistor waveforms obey a power sink characteristic. When $m_a = 0$, then the average power $\langle p(t) \rangle_{T_s}$ is a function only of L, i_c, and f_s. The presence of the artificial ramp causes $\langle p(t) \rangle_{T_s}$ to additionally depend on the converter voltages, via m_1.

The power sink characteristic can also be explained via inductor energy arguments. During the first subinterval, the inductor current increases from 0 to i_{pk}. In the process, the inductor stores the following energy:

$$W = \tfrac{1}{2} L i_{pk}^2 \tag{12.109}$$

The energy W is transferred from the power input v_g, through the switch network input port, to the inductor, once per switching period. This energy transfer process accounts for the power flow

$$\langle p(t) \rangle_{T_s} = W f_s = \tfrac{1}{2} L i_{pk}^2 f_s \tag{12.110}$$

The switch network input port, that is, the transistor terminals, can therefore be modeled by a power sink element, as in Fig. 12.32.

The average switch network output port current, that is, the average diode current, is

$$\langle i_2(t) \rangle_{T_s} = \frac{1}{T_s} \int_t^{t+T_s} i_2(\tau) d\tau = \frac{q_2}{T_s} \tag{12.111}$$

By inspection of Fig. 12.31, the area q_2 is given by

$$q_2 = \tfrac{1}{2} i_{pk} d_2 T_s \tag{12.112}$$

The duty cycle d_2 is determined by the time required for the inductor current to return to zero, during the second subinterval. By arguments similar to those used to derive Eq. (11.12), the duty cycle d_2 can be found as follows:

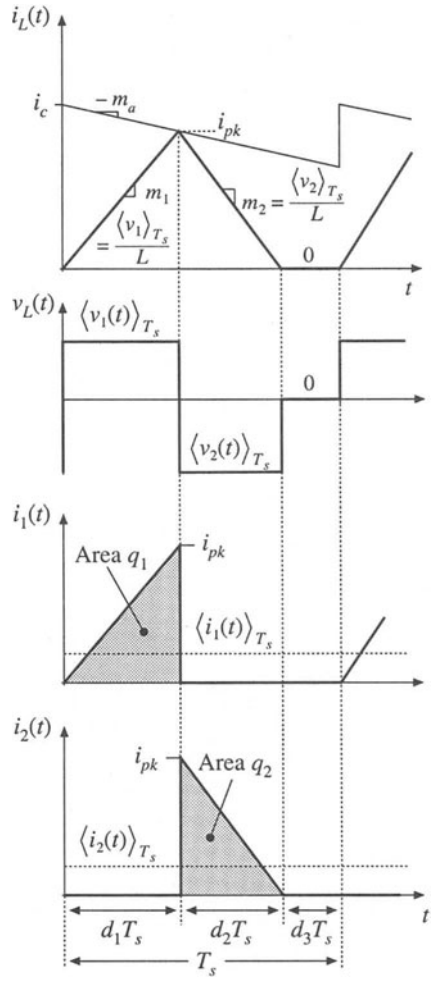

Fig. 12.31 Waveforms, CPM DCM buck–boost example.

$$d_2(t) = d_1(t) \frac{\langle v_1(t) \rangle_{T_s}}{\langle v_2(t) \rangle_{T_s}} \tag{12.113}$$

Substitution of Eqs. (12.113), (12.112), and (12.110) into Eq. (12.111) yields

$$\langle i_2(t) \rangle_{T_s} = \frac{\langle p(t) \rangle_{T_s}}{\langle v_2(t) \rangle_{T_s}} \tag{12.114}$$

The output port of the averaged switch network is therefore described by the relationship

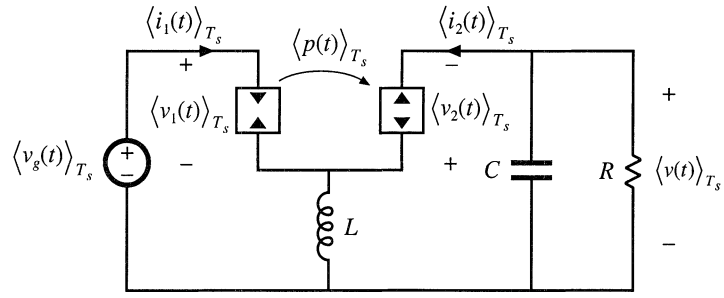

Fig. 12.32 CPM DCM buck–boost converter model, derived via averaged switch modeling.

$$\langle i_2(t)\rangle_{T_s}\langle v_2(t)\rangle_{T_s} = \frac{\frac{1}{2}Li_c^2(t)f_s}{\left(1+\frac{m_a}{m_1}\right)^2} = \langle p(t)\rangle_{T_s} \tag{12.115}$$

In the averaged model, the diode can be replaced by a power source of value $\langle p(t)\rangle_{T_s}$, equal to the power apparently consumed at the switch network input port. During the second subinterval, the inductor releases all of its stored energy through the diode, to the converter output. This results in an average power flow of value $\langle p(t)\rangle_{T_s}$.

A CPM DCM buck-boost averaged model is therefore as given in Fig. 12.32. In this model, the transistor is simply replaced by a power sink of value $\langle p(t)\rangle_{T_s}$, while the diode is replaced by a power source also of value $\langle p(t)\rangle_{T_s}$.

The steady-state equivalent circuit model of the CPM DCM buck-boost converter is obtained by letting the inductor and capacitor tend to short- and open-circuits, respectively. The model of Fig. 12.33 is obtained. The steady-state output voltage V can now be determined by equating the dc load power to the converter average power $\langle p(t)\rangle_{T_s}$. For a resistive load, one obtains

$$\frac{V^2}{R} = P \tag{12.116}$$

where the steady state value of $\langle p(t)\rangle_{T_s}$ is given by

$$P = \frac{\frac{1}{2}LI_c^2(t)f_s}{\left(1+\frac{M_a}{M_1}\right)^2} \tag{12.117}$$

and where I_c is the steady-state value of the control input $i_c(t)$. Solution for V yields the following result

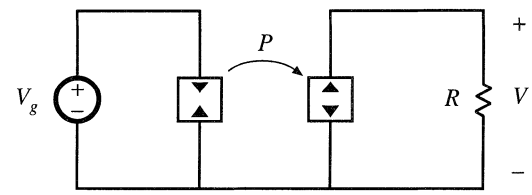

Fig. 12.33 Steady-state model of the CPM DCM buck–boost converter.

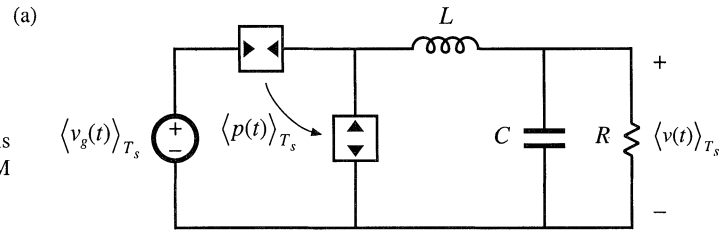

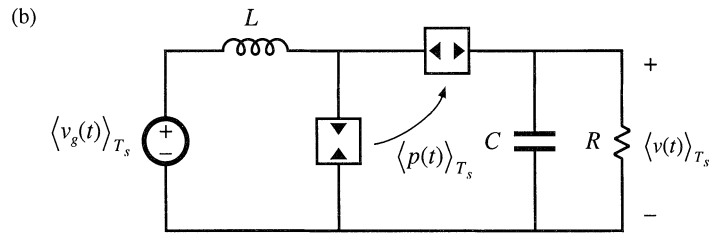

Fig. 12.34 Averaged models of current-programmed DCM converters: (a) buck, (b) boost.

$$V = \sqrt{PR} = I_c \sqrt{\frac{RLf_s}{2\left(1 + \frac{M_a}{M_1}\right)^2}} \tag{12.118}$$

for the case of a resistive load.

Averaged models of the DCM CPM buck, boost, and other converters can be found in a similar manner. In each case, the average transistor waveforms are shown to follow a power sink characteristic, while the average diode waveforms follow a power source characteristic. The resulting equivalent circuits of the CPM DCM buck and boost converters are illustrated in Fig. 12.34. In each case, the average power is given by

Table 12.6 Steady-state DCM current-programmed characteristics of basic converters

Converter	M	I_{crit}	Stability range when $m_a = 0$
Buck	$\frac{P_{load} - P}{P_{load}}$	$\frac{1}{2}\left(I_c - M m_a T_s\right)$	$0 \le M < \frac{2}{3}$
Boost	$\frac{P_{load}}{P_{load} - P}$	$\frac{\left(I_c - \frac{M-1}{M} m_a T_s\right)}{2M}$	$0 \le D \le 1$
Buck–boost	Depends on load characteristic: $P_{load} = P$	$\frac{\left(I_c - \frac{M}{M-1} m_a T_s\right)}{2(M-1)}$	$0 \le D \le 1$

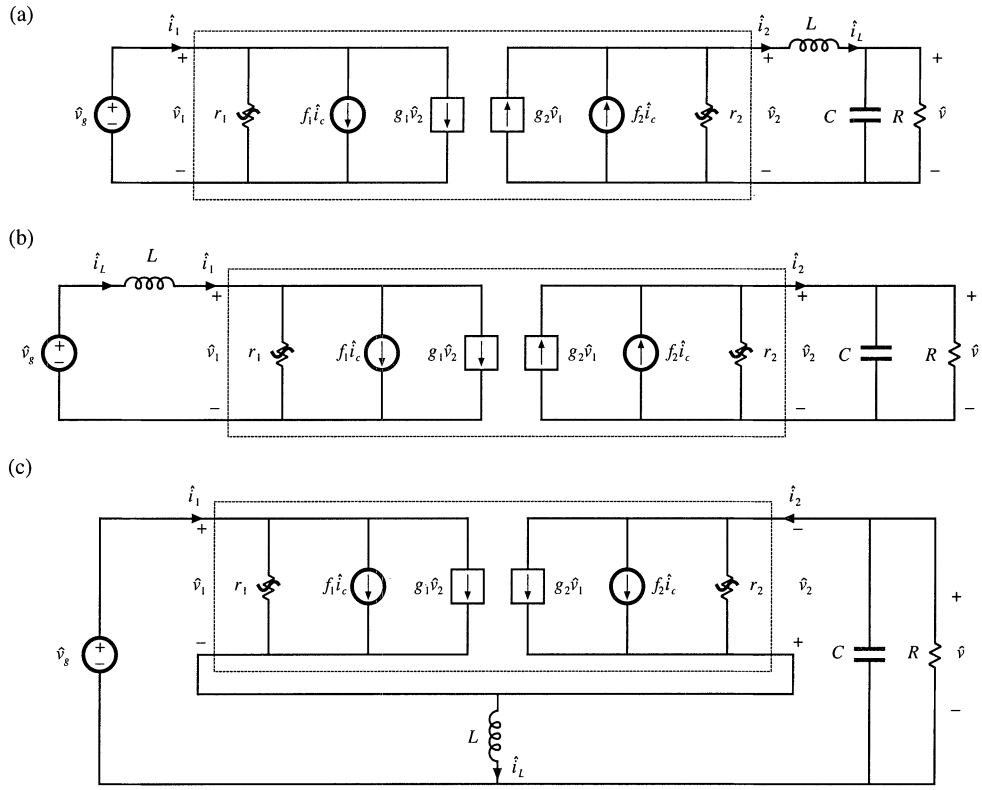

Fig. 12.35 Small-signal models of DCM CPM converters, derived by perturbation and linearization of Figs. 12.32 and 12.34: (a) buck, (b) boost, (c) buck–boost.

$$\langle p(t)\rangle_{T_s} = \frac{\frac{1}{2}Li_c^2(t)f_s}{\left(1+\frac{m_a}{m_1}\right)^2} \tag{12.119}$$

with m_1 defined as in Eq. (12.1).

Steady-state characteristics of the DCM CPM buck, boost, and buck–boost converters are summarized in Table 12.6. In each case, the dc load power is $P_{load} = VI$ and P is given by Eq. (12.117). The conditions for operation of a current programmed converter in the discontinuous conduction mode can be expressed as follows:

$$\begin{aligned} |I| &> |I_{crit}| \quad \text{for CCM} \\ |I| &< |I_{crit}| \quad \text{for DCM} \end{aligned} \tag{12.120}$$

where I is the dc load current. The critical load current at the CCM–DCM boundary, I_{crit}, is expressed as a function of I_c and the voltage conversion ratio $M = V/V_g$ in Table 12.6.

In the discontinuous conduction mode, the inductor current is zero at the beginning and end of

Table 12.7 Current programmed DCM small-signal equivalent circuit parameters: input port

Converter	g_1	f_1	r_1
Buck	$\frac{1}{R}\left(\frac{M^2}{1-M}\right)\frac{\left(1-\frac{m_a}{m_1}\right)}{\left(1+\frac{m_a}{m_1}\right)}$	$2\frac{I_1}{I_c}$	$-R\left(\frac{1-M}{M^2}\right)\frac{\left(1+\frac{m_a}{m_1}\right)}{\left(1-\frac{m_a}{m_1}\right)}$
Boost	$-\frac{1}{R}\left(\frac{M}{M-1}\right)$	$2\frac{I}{I_c}$	$\frac{R}{M^2\left(\frac{2-M}{M-1}+\frac{2m_a/m_1}{1+\frac{m_a}{m_1}}\right)}$
Buck–boost	0	$2\frac{I_1}{I_c}$	$\frac{-R}{M^2}\frac{\left(1+\frac{m_a}{m_1}\right)}{\left(1-\frac{m_a}{m_1}\right)}$

Table 12.8 Current programmed DCM small-signal equivalent circuit parameters: output port

Converter	g_2	f_2	r_2
Buck	$\frac{1}{R}\left(\frac{M}{1-M}\right)\frac{\left(\frac{m_a}{m_1}(2-M)-M\right)}{\left(1+\frac{m_a}{m_1}\right)}$	$2\frac{I}{I_c}$	$R\frac{(1-M)\left(1+\frac{m_a}{m_1}\right)}{\left(1-2M+\frac{m_a}{m_1}\right)}$
Boost	$\frac{1}{R}\left(\frac{M}{M-1}\right)$	$2\frac{I_2}{I_c}$	$R\left(\frac{M-1}{M}\right)$
Buck–boost	$\frac{2M}{R}\frac{\left(\frac{m_a}{m_1}\right)}{\left(1+\frac{m_a}{m_1}\right)}$	$2\frac{I_2}{I_c}$	R

each switching period. As a result, the current programmed controller does not exhibit the type of instability described in Section 12.1. The current programmed controllers of DCM boost and buck–boost converters are stable for all duty cycles with no artificial ramp. However, the CPM DCM buck converter exhibits a different type of low-frequency instability when $M > 2/3$ and $m_a = 0$, that arises because the dc output characteristic is nonlinear and can exhibit two equilibrium points when the converter drives a resistive load. The stability range can be extended to $0 \le D \le 1$ by addition of an artificial ramp having slope $m_a > 0.086\, m_2$, or by addition of output voltage feedback.

Small-signal models of DCM CPM converters can be derived by perturbation and linearization of the averaged models of Figs. 12.32 and 12.34. The results are given in Fig. 12.35. Parameters of the small-signal models are listed in Tables 12.7 and 12.8.

The CPM DCM small-signal models of Fig. 12.35 are quite similar to the respective small-signal models of DCM duty-ratio controlled converters illustrated in Figs. 11.15 and 11.17. The sole differences are the parameter expressions of Tables 12.7 and 12.8. Transfer functions can be determined in a

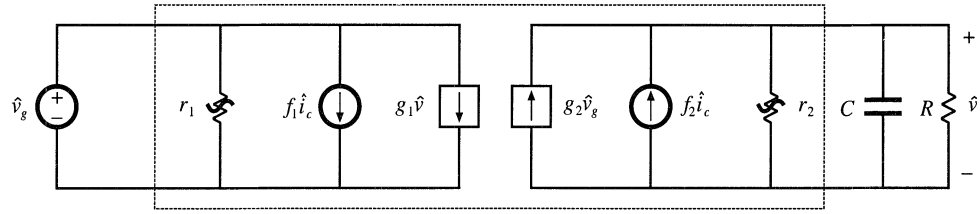

Fig. 12.36 Simplified small-signal model obtained by letting L become zero in Fig. 12.35 (a), (b), or (c).

similar manner. In particular, a simple approximate way to determine the low-frequency small-signal transfer functions of the CPM DCM buck, boost, and buck-boost converters is to simply let the inductance L tend to zero in the equivalent circuits of Fig. 12.35. This approximation is justified for frequencies sufficiently less than the converter switching frequency, because in the discontinuous conduction mode the value of L is small, and hence the pole and any RHP zero associated with L occur at frequencies near to or greater than the switching frequency. For all three converters, the equivalent circuit of Fig. 12.36 is obtained.

Figure 12.36 predicts that the control-to-output transfer function $G_{vc}(s)$ is

$$G_{vc}(s) = \left.\frac{\hat{v}}{\hat{i}_c}\right|_{\hat{v}_g = 0} = \frac{G_{c0}}{1 + \frac{s}{\omega_p}} \tag{12.121}$$

with

$$G_{c0} = f_2\left(R \| r_2\right)$$
$$\omega_p = \frac{1}{\left(R \| r_2\right) C}$$

The line-to-output transfer function is predicted to be

$$G_{vg}(s) = \left.\frac{\hat{v}}{\hat{v}_g}\right|_{\hat{i}_c = 0} = \frac{G_{g0}}{1 + \frac{s}{\omega_p}} \tag{12.122}$$

with

$$G_{g0} = g_2\left(R \| r_2\right)$$

If desired, more accurate expressions which account for inductor dynamics can be derived by solution of the models of Fig. 12.35.

12.5 SUMMARY OF KEY POINTS

1. In current-programmed control, the peak switch current $i_s(t)$ follows the control input $i_c(t)$. This widely used control scheme has the advantage of a simpler control-to-output transfer function. The line-to-output transfer functions of current-programmed buck converters are also reduced.

2. The basic current-programmed controller is unstable when $D > 0.5$, regardless of the converter topology. The controller can be stabilized by addition of an artificial ramp having slope m_a. When $m_a > 0.5m_2$, then the controller is stable for all duty cycles.

3. The behavior of current-programmed converters can be modeled in a simple and intuitive manner by the first-order approximation $\langle i_L(t) \rangle_{T_s} \approx i_c(t)$. The averaged terminal waveforms of the switch network can then be modeled simply by a current source of value i_c, in conjunction with a power sink or power source element. Perturbation and linearization of these elements leads to the small-signal model. Alternatively, the small-signal converter equations derived in Chapter 7 can be adapted to cover the current programmed mode, using the simple approximation $i_L(t) \approx i_c(t)$.

4. The simple model predicts that one pole is eliminated from the converter line-to-output and control-to-output transfer functions. Current programming does not alter the transfer function zeroes. The dc gains become load-dependent.

5. The more accurate model of Section 12.3 correctly accounts for the difference between the average inductor current $\langle i_L(t) \rangle_{T_s}$ and the control input $i_c(t)$. This model predicts the nonzero line-to-output transfer function $G_{vg}(s)$ of the buck converter. The current-programmed controller behavior is modeled by a block diagram, which is appended to the small-signal converter models derived in Chapter 7. Analysis of the resulting multiloop feedback system then leads to the relevant transfer functions.

6. The more accurate model predicts that the inductor pole occurs at the crossover frequency f_c of the effective current feedback loop gain $T_i(s)$. The frequency f_c typically occurs in the vicinity of the converter switching frequency f_s. The more accurate model also predicts that the line-to-output transfer function $G_{vg}(s)$ of the buck converter is nulled when $m_a = 0.5m_2$.

7. Current programmed converters operating in the discontinuous conduction mode are modeled in Section 12.4. The averaged transistor waveforms can be modeled by a power sink, while the averaged diode waveforms are modeled by a power source. The power is controlled by $i_c(t)$. Perturbation and linearization of these averaged models, as usual, leads to small-signal equivalent circuits.

REFERENCES

[1] C. DEISCH, "Simple Switching Control Method Changes Power Converter into a Current Source," *IEEE Power Electronics Specialists Conference*, 1978 Record, pp. 300-306.

[2] A. CAPEL, G. FERRANTE, D. O'SULLIVAN, and A. WEINBERG, "Application of the Injected Current Model for the Dynamic Analysis of Switching Regulators with the New Concept of LC^3 Modulator," *IEEE Power Electronics Specialists Conference*, 1978 Record, pp. 135-147.

[3] S. HSU, A. BROWN, L. RENSINK, and R. D. MIDDLEBROOK, "Modeling and Analysis of Switching Dc-to-Dc Converters in Constant-Frequency Current Programmed Mode," *IEEE Power Electronics Specialists Conference*, 1979 Record, pp. 284-301.

[4] F. C. LEE and R. A. CARTER, "Investigations of Stability and Dynamic Performances of Switching Regulators Employing Current-Injected Control," *IEEE Power Electronics Specialists Conference*, 1981 Record, pp. 3-16.

[5] R. D. MIDDLEBROOK, "Topics in Multiple-Loop Regulators and Current-Mode Programming," *IEEE Power Electronics Specialists Conference*, 1985 Record, pp. 716-732.

[6] R. D. MIDDLEBROOK, "Modeling Current Programmed Buck and Boost Regulators," *IEEE Transactions on Power Electronics*, Vol. 4, No. 1, January 1989, pp. 36-52.

[7] G. VERGHESE, C. BRUZOS, and K. MAHABIR, "Averaged and Sampled-Data Models for Current Mode Control: A Reexamination," *IEEE Power Electronics Specialists Conference*, 1989 Record, pp. 484-491.

[8] D. M. MITCHELL, *Dc–Dc Switching Regulator Analysis*, New York: McGraw-Hill, 1988, Chapter 6.

[9] A. KISLOVSKI, R. REDL, and N. SOKAL, *Dynamic Analysis of Switching-Mode DC/DC Converters,* New York: Van Nostrand Reinhold, 1994.

[10] A. BROWN and R. D. MIDDLEBROOK, "Sampled-Data Modeling of Switching Regulators," *IEEE Power Electronics Specialists Conference*, 1981 Record, pp. 716-732.

[11] R. RIDLEY, "A New Continuous-Time Model for Current-Mode Control," *IEEE Transactions on Power Electronics*, Vol. 6, No. 2, April 1991, pp. 271-280.

[12] F. D. TAN and R. D. MIDDLEBROOK, "Unified Modeling and Measurement of Current-Programmed Converters," *IEEE Power Electronics Specialists Conference*, 1993 Record, pp. 380-387.

[13] R. TYMERSKI, "Sampled-Data Modeling of Switched Circuits, Revisited," *IEEE Power Electronics Specialists Conference*, 1993 Record, pp. 395-401.

[14] W. TANG, F. C. LEE, R. B. RIDLEY and I. COHEN, "Charge Control: Modeling, Analysis and Design," *IEEE Power Electronics Specialists Conference*, 1992 Record, pp. 503-511.

[15] K. SMEDLEY and S. ĆUK, "One-Cycle Control of Switching Converters," *IEEE Power Electronics Specialists Conference*, 1991 Record, pp. 888-896.

PROBLEMS

12.1 A nonideal buck converter operates in the continuous conduction mode, with the values $V_g = 10$ V, $f_2 = 100$ kHz, $L = 4$ μH, $C = 75$ μF, and $R = 0.25$ Ω. The desired full-load output is 5 V at 20 A. The power stage contains the following loss elements: MOSFET on-resistance $R_{on} = 0.1$ Ω, Schottky diode forward voltage drop $V_D = 0.5$ V, inductor winding resistance $R_L = 0.03$ Ω.

(a) Steady-state analysis: determine the converter steady-state duty cycle D, the inductor current ripple slopes m_1 and m_2, and the dimensionless parameter $K = 2L/RT_s$.

(b) Determine the small-signal equations for this converter, for duty cycle control.

A current-programmed controller is now implemented for this converter. An artificial ramp is used, having a fixed slope $M_a = 0.5M_2$, where M_2 is the steady-state slope m_2 obtained with an output of 5 V at 20 A.

(c) Over what range of D is the current programmed controller stable? Is it stable at rated output? Note that the nonidealities affect the stability boundary.

(d) Determine the control-to-output transfer function $G_{vc}(s)$, using the simple approximation $\langle i_L(t) \rangle_{T_s} \approx i_c(t)$. Give analytical expressions for the corner frequency and dc gain. Sketch the Bode plot of $G_{vc}(s)$.

12.2 Use the averaged switch modeling approach to model the CCM boost converter with current-programmed control:

(a) Define the switch network terminal quantities as in Fig. 7.46(a). With the assumption that $\langle i_L(t) \rangle_{T_s} \approx i_c(t)$, determine expressions for the average values of the switch network terminal waveforms, and hence derive the equivalent circuit of Fig. 12.18(a).

(b) Perturb and linearize your model of part (a), to obtain the equivalent circuit of Fig. 12.22.

(c) Solve your model of part (b), to derive expressions for the control-to-output transfer function $G_{vc}(s)$ and the line-to-output transfer function $G_{vg}(s)$. Express your results in standard normalized form, and give analytical expressions for the corner frequencies and dc gains.

12.3 Use the averaged switch modeling approach to model the CCM Ćuk converter with current-programmed control. A Ćuk converter is diagrammed in Fig. 2.20.

(a) It is desired to model the switch network with an i_c current source and a dependent power source or sink, using the approach of Section 12.2.2. How should the switch network terminal voltages and currents be defined?

(b) Sketch the switch network terminal voltage and current waveforms. With the assumption that $\langle i_1(t)\rangle_{T_s} - \langle i_2(t)\rangle_{T_s} \approx i_c(t)$ (where i_1 and i_2 are the inductor currents defined in Fig. 2.20), determine expressions for the average values of the switch network terminal waveforms, and hence derive an equivalent circuit similar to the equivalent circuits of Fig. 12.18.

(c) Perturb and linearize your model of part (b), to obtain a small signal equivalent circuit similar to the model of Fig. 12.19. It is not necessary to solve your model.

12.4 The full-bridge converter of Fig. 6.19(a) operates with $V_g = 320$ V, and supplies 1000 W to a 42 V resistive load. Losses can be neglected, the duty cycle is 0.7, and the switching period T_s defined in Fig. 6.20 is 10 μsec. $L = 50$ μH and $C = 100$ μF. A current-programmed controller is employed, whose waveforms are referred to the secondary side of the transformer. In the following calculations, you may neglect the transformer magnetizing current.

(a) What is the minimum artificial ramp slope m_a that will stabilize the controller at the given operating point? Express your result in terms of m_2.

(b) An artificial ramp having the slope $m_a = m_2$ is employed. Sketch the Bode plot of the current loop gain $T_i(s)$, and label numerical values of the corner frequencies and dc gains. It is not necessary to re-derive the analytical expression for T_i. Determine the crossover frequency f_c.

(c) For $m_a = m_2$, sketch the Bode plots of the control-to-output transfer function $G_{vc}(s)$ and line-to-output transfer function $G_{vg}(s)$, and label numerical values of the corner frequencies and dc gains. It is not necessary to re-derive analytical expressions for these transfer functions.

12.5 In a CCM current-programmed buck converter, it is desired to minimize the line-to-output transfer function $G_{vg}(s)$ via the choice $m_a = 0.5m_2$. However, because of component tolerances, the value of inductance L can vary by ±10% from its nominal value of 100 μH. Hence, m_a is fixed in value while m_2 varies, and $m_a = 0.5m_2$ is obtained only at the nominal value of L. The switching frequency is 100 kHz, the output voltage is 15 V, the load current varies over the range 2 to 4 A, and the input voltage varies over the range 22 to 32 V. You may neglect losses. Determine the worst-case (maximum) value of the line-to-output dc gain $G_{vg}(0)$.

12.6 The nonideal flyback converter of Fig. 7.18 employs current-programmed control, with artificial ramp having slope m_a. MOSFET Q_1 exhibits on-resistance R_{on}. All current programmed controller waveforms are referred to the transformer primary side.

(a) Derive a block diagram which models the current-programmed controller, of form similar to Fig. 12.24. Give analytical expressions for the gains in your block diagram.

(b) Combine your result of part (a) with the converter small-signal model. Derive a new expression for the control-to-output transfer function $G_{vc}(s)$.

12.7 A buck converter operates with current-programmed control. The element values are:

$V_g = 120$ V	$D = 0.6$
$R = 10$ Ω	$f_s = 100$ kHz
$L = 550$ μH	$C = 100$ μF

An artificial ramp is employed, having slope 0.15 A/μsec.

(a) Construct the magnitude and phase asymptotes of the control-to-output transfer function $G_{vd}(s)$ for duty-cycle control. On the same plot, construct the magnitude and phase asymptotes of the control-to-output transfer function $G_{vc}(s)$ for current-programmed control. Compare.

(b) Construct the magnitude asymptotes of the line-to-output transfer function $G_{vg}(s)$ for duty-cycle control. On the same plot, construct the magnitude asymptotes of the line-to-output transfer function $G_{vg\text{-}cpm}(s)$ for current-programmed control. Compare.

12.8 A buck-boost converter operates in the discontinuous conduction mode. Its current-programmed controller has no compensating artificial ramp: $m_a = 0$.

(a) Derive an expression for the control-to-output transfer function $G_{vc}(s)$, using the approximation $L \approx 0$. Give analytical expressions for the corner frequency and dc gain.

(b) Repeat part (a), with the inductor included. Show that, provided the inductor is sufficiently small, then the inductor merely adds a high-frequency pole and zero to $G_{vc}(s)$, and the low-frequency pole derived in part (a) is essentially unchanged.

(c) At the CCM-DCM boundary, what is the minimum value of the RHP zero frequency?

12.9 A current-programmed boost converter interfaces a 3 V battery to a small portable 5 V load. The converter operates in the discontinuous conduction mode, with constant transistor on-time t_{on} and variable off-time; the switching frequency can therefore vary and is used as the control variable. There is no artificial ramp, and the peak transistor current i_c is equal to a fixed value I_c; in practice, I_c is chosen to minimize the total loss.

(a) Sketch the transistor and diode voltage and current waveforms. Determine expressions for the waveform average values, and hence derive a large-signal averaged equivalent circuit for this converter.

(b) Perturb and linearize your model of part (a), to obtain a small-signal equivalent circuit. Note that the switching frequency f_s should be perturbed.

(c) Solve your model of part (b), to derive an expression for the low-frequency control-to-output transfer function $G_{vf}(s) = \hat{v}(s)/\hat{f}_s(s)$. Express your results in standard normalized form, and give analytical expressions for the corner frequencies and dc gains. You may assume that L is small.

12.10 A current-programmed boost converter is employed in a low-harmonic rectifier system, in which the input voltage is a rectified sinusoid: $v_g(t) = V_M \mid \sin(\omega t) \mid$. The dc output voltage is $v(t) = V > V_M$. The capacitance C is large, such that the output voltage contains negligible ac variations. It is desired to control the converter such that the input current $i_g(t)$ is proportional to $v_g(t)$: $i_g(t) = v_g(t)/R_e$, where R_e is a constant, called the "emulated resistance." The averaged boost converter model of Fig. 12.18(a) suggests that this can be accomplished by simply letting $i_c(t)$ be proportional to $v_g(t)$, according to $i_c(t) = v_g(t)/R_e$. You may make the simplifying assumption that the converter always operates in the continuous conduction mode.

(a) Solve the model of Fig. 12.18(a), subject to the assumptions listed above, to determine the power $\langle p(t) \rangle_{T_s}$. Find the average value of $\langle p(t) \rangle_{T_s}$, averaged over one cycle of the ac input $v_g(t)$.

(b) An artificial ramp is necessary to stabilize the current-programmed controller at some operating points. What is the minimum value of m_a that ensures stability at all operating points along the input rectified sinusoid? Express your result as a function of V and L. Show your work.

(c) The artificial ramp and inductor current ripple cause the average input current to differ from $i_c(t)$. Derive an algebraic expression for $\langle i_g(t) \rangle_{T_s}$, as a function of $i_c(t)$ and other quantities such as m_a, $v_g(t)$, V, L, and T_s. For this part, you may assume that the inductor dynamics are negligible. Show your work.

(d) Substitute $v_g(t) = V_M \mid \sin(\omega t) \mid$ and $i_c(t) = v_g(t)/R_e$, into your result of part (c), to determine an expression for $i_g(t)$. How does $i_g(t)$ differ from a rectified sinusoid?

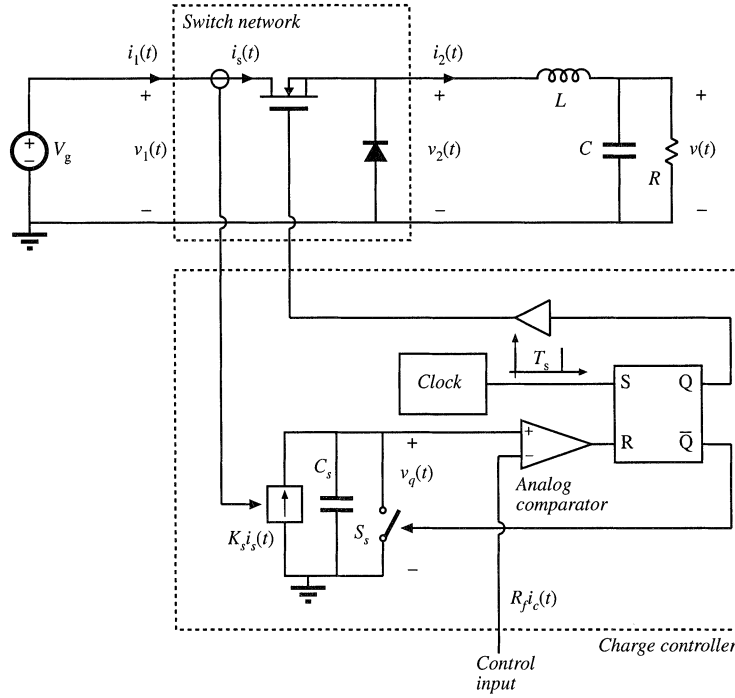

Fig. 12.37 Buck converter with charge controller, Problem 12.11.

12.11 Figure 12.37 shows a buck converter with a charge controller [14]. Operation of the charge controller is similar to operation of the current-programmed controller. At the beginning of each switching period, at time $t = 0$, a short clock pulse sets the SR latch. The logic high signal at the Q output of the latch turns the power MOSFET on. At the same time, the logic low signal at the $\overline{Q}$ output of the latch turns the switch S_s off. Current $K_s i_s$ proportional to the power MOSFET current charges the capacitor C_s. At $t = dT_s$, the capacitor voltage $v_q(t)$ reaches the control input voltage $R_f i_c$, the comparator output goes high and resets the latch. The logic low signal at the Q output of the latch turns the power MOSFET off. At the same time, the logic high signal at the $\overline{Q}$ output of the latch turns the switch S_s on, which quickly discharges the capacitor C_s to zero.

In this problem, the converter and controller parameters are: $V_g = 24$ V, $f_s = 1/T_s = 100$ kHz, $L = 60$ μH, $C = 100$ μF, $R = 3\ \Omega$, $K_s T_s / C_s = R_f = 1\ \Omega$. You can assume that the converter operates in continuous conduction mode.

(a) Find expressions for the average values of the switch network terminal waveforms, and hence derive a large-signal averaged switch model of the buck switch network with charge control. The control input to the model is the control current i_c. The averaged switch model should consist of a current source and a power source. The switch duty cycle d should not appear in the model.

(b) Using the averaged switch model derived in part (a), find an expression for the quiescent output voltage V as a function of V_g, I_c, and R. Given $I_c = 2$ A, find numerical values for V, I_1, I_2, and the duty cycle D. For this quiescent operating point, sketch the waveforms $i_1(t)$, $i_2(t)$, and $v_q(t)$ during one switching period.

(c) Perturb and linearize the averaged switch model from part (a) to derive a small-signal averaged switch model for the buck switch network with charge control. Find analytical expressions for

all parameter values in terms of the converter parameters and the quiescent operating conditions. Sketch the complete small-signal model of the buck converter with the charge controller.

(d) Solve the model obtained in part (c) to find the control-to-output transfer function $G_{vc}(s) = \hat{v}/\hat{t}_c$. At the quiescent operating point found in part (b), construct the Bode plot for the magnitude of G_{vc} and label all salient features of the magnitude response.

(e) Comment on advantages charge control may have compared to duty-cycle control or current-programmed control.

12.12 Figure 12.38 shows a buck converter with a one-cycle controller [15]. Operation of the one-cycle controller is similar to operation of the current-programmed controller. At the beginning of each switching period, at time $t = 0$, a short clock pulse sets the SR latch. The logic high signal at the Q output of the latch turns the power MOSFET on. At the same time, the logic low signal at the $\overline{Q}$ output of the latch turns the switch S_s off. Current $G_s v_2(t)$ proportional to the voltage $v_2(t)$ charges the capacitor C_s. At $t = dT_s$, the capacitor voltage $v_s(t)$ reaches the control input voltage v_c, the comparator output goes high and resets the latch. The logic low signal at the Q output of the latch turns the power MOSFET off. At the same time, the logic high signal at the $\overline{Q}$ output of the latch turns the switch S_s on, which quickly discharges the capacitor C_s to zero.

In this problem, the converter and controller parameters are: $V_g = 24$ V, $f_s = 1/T_s = 100$ kHz, $L = 60$ μH, $C = 100$ μF, $R = 3\ \Omega$, $G_s T_s / C_s = 1$. You can assume that the converter operates in the continuous conduction mode.

(a) Find expressions for the average values of the switch network terminal waveforms, and hence derive a large-signal averaged switch model of the buck switch network with one-cycle control. The control input to the model is the control voltage v_c. The switch duty cycle d should not appear in the model.

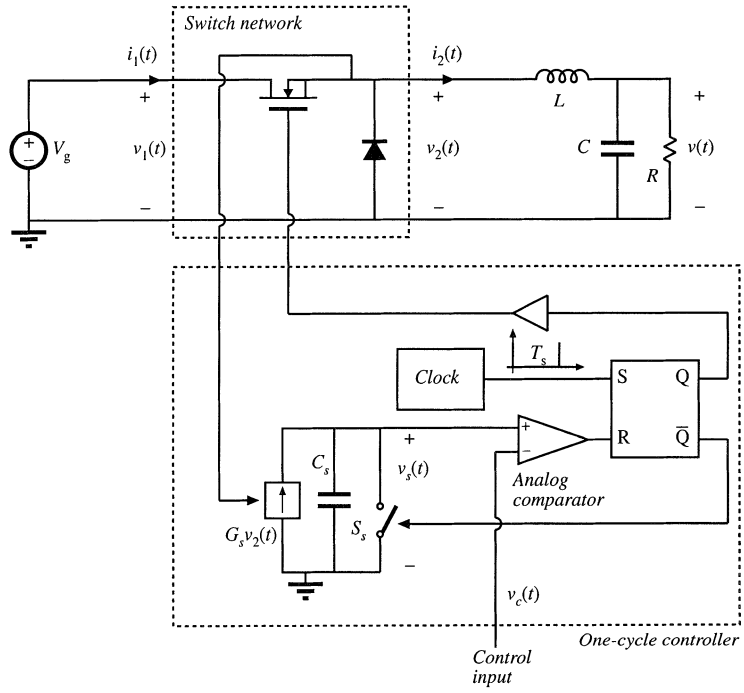

Fig. 12.38 Buck converter with one-cycle controller, Problem 12.12.

(b) Using the averaged switch model derived in part (a), find an expression for the quiescent output voltage V as a function of V_c. Given $V_c = 10$ V, find the numerical values for V, I_1, I_2, and the duty cycle D. For this quiescent operating point, sketch the waveforms $i_1(t)$, $i_2(t)$, and $v_s(t)$ during one switching period.

(c) Perturb and linearize the averaged switch model from part (a) to derive a small-signal averaged switch model for the buck switch network with one-cycle control. Find analytical expressions for all parameter values in terms of the converter parameters and the quiescent operating conditions. Sketch the complete small-signal model of the buck converter with the one-cycle controller.

(d) Solve the model obtained in part (c) to find the control-to-output transfer function $G_{vc}(s) = \hat{v}/\hat{v}_c$, and the line-to-output transfer function $G_{vg}(s) = \hat{v}/\hat{v}_g$. For the quiescent operating point found in part (b), sketch the magnitude Bode plots of these transfer functions, and label all salient features.

(e) Comment on advantages one-cycle control may have compared to duty-cycle control.